

Landau levels of molecules: Angular-momentum coupling between cyclotron motion and core rotation

Yasuyuki Kimura*

Department of Electrical Engineering, Faculty of Science and Engineering, Doshisha University, 1-3 Tatara Miyakodani, Kyotanabe 610-0321, Japan

Ken Takazawa

National Institute for Materials Science, 3-13 Sakura, Tsukuba 305-0003, Japan

(Received 6 June 2013; revised manuscript received 14 January 2014; published 24 February 2014)

In a high magnetic field of 3–7 T, nitric oxide (NO) molecules are excited by the double-resonance method through the intermediate $A^2\Sigma^+F_1(v''=0, N''=0)$ level to the Landau levels in the energy region above the zero-field ionization limit to the $\text{NO}^+ X^1\Sigma^+(v^+=0, N^+=0)$ ion. By detecting NO^+ ions, the photoionization cross section through the Landau levels is determined as a function of the second laser's frequency. The cross section contains broad structures and fine structures. Fourier analysis of the cross section and classical trajectory calculations of the Rydberg electron demonstrate that the broad structure is formed by the Landau level generated by the cyclotron motion of the electron around the $N^+=0$ core in a plane perpendicular to the field, while the fine structure is formed by the Landau level generated by the three-dimensional cyclotron motion around the excited $N^+=2$ core. By simulating the energy structure of the Landau level, the electron's orbital angular momentum is confirmed to be decoupled from the core rotation in the Landau levels. From the selection rules of the excitation, it is demonstrated that the Landau levels with the $N^+=0$ core are excited using the s character in the $A^2\Sigma^+$ state, while those with the $N^+=2$ core are excited using the d character. The dominant partial wave, thus determined, explains well the starting direction of the classical trajectory.

DOI: [10.1103/PhysRevA.89.023427](https://doi.org/10.1103/PhysRevA.89.023427)

PACS number(s): 33.80.Eh, 33.80.Rv, 32.60.+i

I. INTRODUCTION

The effects of a magnetic field on the structure and dynamics of atoms and molecules have evoked continuous interest for several decades. For explaining these effects, Fig. 1 schematically shows the energy structure of a Rydberg atom. In a zero field [Fig. 1(a)], the l levels are nearly degenerate and the level energy is given by $-\mathcal{R}/n^2$, where n is the principal quantum number and \mathcal{R} is the Rydberg constant. Distribution of the closed classical trajectories (Kepler orbits) of the ensemble is spherically symmetrical in a Coulomb field. In a low magnetic field of less than approximately 1 T, the Lorentz force acting on their electrons is several orders of magnitude weaker than the Coulomb binding force. The external field acts as a perturbation. In this case, the linear Zeeman effect is observed, which is induced by the paramagnetic term $\mu_B B(l_Z + 2S_Z)/\hbar$. Here the space-fixed Z axis is parallel to the magnetic field of strength B , μ_B is the Bohr magneton, \hbar is the Planck's constant, and l_Z and S_Z are the Z components of the electron's orbital angular-momentum l and the electron spin S . The diamagnetic term $(e^2 B^2/8m)r^2 \sin^2 \theta$ dominates the paramagnetic term for higher B or for high Rydberg states, where e is the elementary electric charge, m is the mass of an electron, and r, θ are the spherical coordinates of an electron.

For atoms, the quadratic Zeeman effect, which is induced by the diamagnetic term, was observed in highly excited alkali-metal atoms in a field of 2.7 T [1]. The diamagnetic term mixes high l levels ($l \geq 3$) at lower n levels, all l levels at higher n levels, and also n levels at far higher levels [2]. The

energy structure is schematically shown in Fig. 1(b). Many experimental [2,3] and theoretical studies [4–8] have reported the quadratic Zeeman effect. As the magnetic field increases further and dominates the Coulomb binding field, which is realized by a field of a several ~ 10 T for high Rydberg atoms, the motion of a high Rydberg electron becomes similar to cyclotron motion around the core. The quantized energy levels thus formed by the diamagnetic term are called Landau levels. The Landau levels spread to the energy region above the zero-field ionization limit because of the Lorentz force, that is, the diamagnetic term. The positive-energy Landau level was first observed with Ba atoms in a field of 2.5 T [9]. Many experiments followed and confirmed that the energy spacing of the Landau levels is $1.5 \hbar \omega_c$ at the zero-field ionization limit and decreases to $\hbar \omega_c$ as the level energy increases to $+\infty$ [10–14], where $\omega_c = eB/m$ is the cyclotron frequency. This variation in the energy spacing was theoretically explained by application of the one-dimensional Bohr-Sommerfeld quantization condition [15] or by wave packet calculation [16] of the Rydberg electron's motion, which was considered to be rotation around the core in a plane perpendicular to the field. The limit of infinite positive energy indicates the case that a free electron is moving in a magnetic field. Thus, the electron rotates with ω_c , and the corresponding energy levels are separated by intervals of $\hbar \omega_c$ (pure Landau level) [15]. At this limit, many Landau levels are degenerate [17]. The energy structure is schematically shown in Fig. 1(e) together with the closed classical trajectories which are in a plane perpendicular to the field.

At around the zero-field ionization limit, a new type of Landau levels was observed, having energy spacings of $0.64 \hbar \omega_c$, $0.39 \hbar \omega_c$, $0.28 \hbar \omega_c$, etc. These Landau levels are associated

*yakimura@mail.doshisha.ac.jp

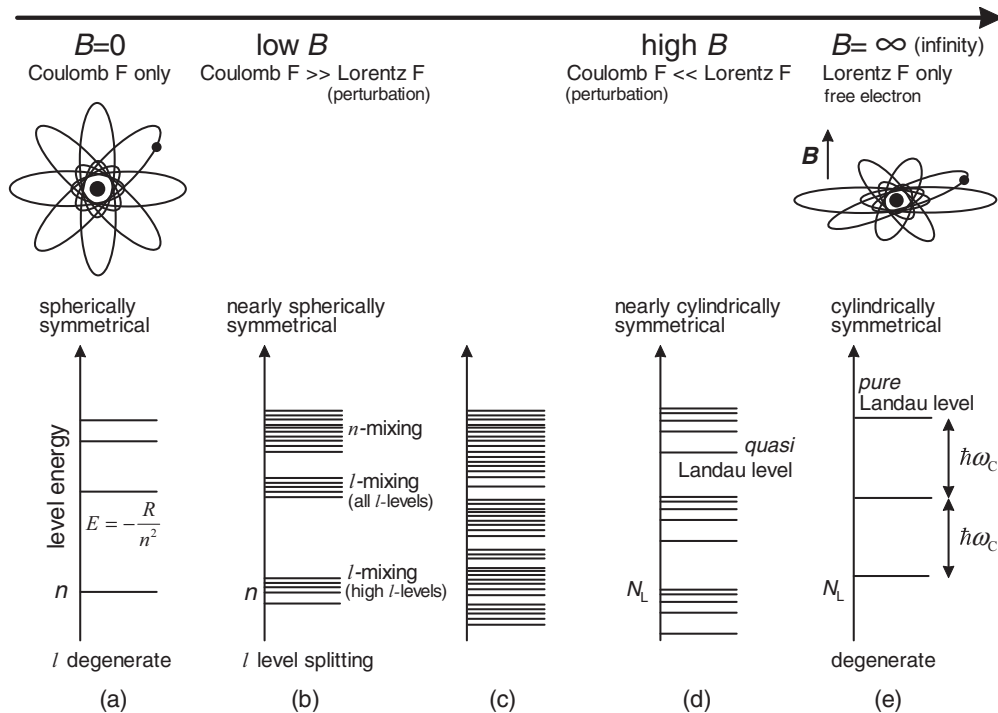


FIG. 1. Energy diagrams of one m_l sublevel of a Rydberg atom in a magnetic field of various strength are shown schematically in order to explain the energy structure of the Landau level. (a) In a zero field, l levels are nearly degenerate and the level energy is given by $-R/n^2$. Closed classical trajectories (Kepler orbits) of the ensemble are shown. Distribution of the trajectories is spherically symmetrical in a Coulomb field. The radius of the state is given by $a_B n^2$ (a_B : Bohr radius). (b) In a low magnetic field, which means that the Lorentz force acting on the electron is far weaker than the Coulomb binding force, the magnetic field acts as a perturbation. At lower n levels, nonpenetrating high l levels ($l \geq 3$) are mixed and their degeneracy is removed by the quadratic Zeeman effect. At higher n levels, all l levels are mixed. At far higher levels, n levels are mixed. (c) Energy structure at an intermediate magnetic field strength between (b) and (d). (d) In a high magnetic field, which means that the Lorentz force is far stronger than the Coulomb force, Rydberg levels converge to many limits that correlate to the pure Landau levels shown in (e). These Rydberg levels are known as quasi Landau levels. The Coulomb force acts as a perturbation which remove the degeneracy of the pure Landau level. (e) In a limit of infinitely high magnetic field, the pure Landau levels are separated by equal energy intervals of $\hbar\omega_c$. Many Landau levels are degenerate. These levels correspond to the cyclotron motion of a free electron. Closed classical trajectories of the ensemble are shown. These trajectories are in a plane perpendicular to the magnetic field ($v = 1$ trajectory in Fig. 6). Distribution of the trajectories is cylindrically symmetrical around the magnetic field.

with various three-dimensional closed classical trajectories of the Rydberg electron [18–26]. Oscillator strengths to these Landau levels were calculated by full quantum-mechanical treatments and correspondence between the Landau level and the closed classical trajectory was clarified [17,27,28]. At the zero-field ionization limit, the Rydberg electron is restricted by dominant Lorentz force and weak Coulomb force. Since the Coulomb force acts as a perturbation, degeneracy of the Landau levels shown in Fig. 1(e) is partly removed. The resultant energy structure is schematically shown in Fig. 1(d) (quasi Landau level). These perturbed levels correspond to the three-dimensional classical trajectories. The relation between the energy structure shown in Figs. 1(d) and 1(e) is similar to those shown in Figs. 1(b) and 1(a). That is to say, the magnetic field is the perturbation for Fig. 1(b), while the Coulomb field is the perturbation for Fig. 1(d). Many studies on atoms are reviewed in Refs. [29–33].

For molecules, however, the high external magnetic field competes with not only the Coulomb binding field but also the electric field between the nuclei (the “intramolecular field”). Therefore, energy structure and dynamics are complicated in a magnetic field even for diatomic molecules, which are

the simplest molecules. Hereafter, the discussion will be limited to diatomic molecules and their Rydberg states. The orbital angular-momentum l of an electron is coupled to the internuclear axis for low n and low l levels [Hund’s case (a) or (b), see inset (A) in Fig. 2]. As n increases, the intramolecular field becomes less dominant, and l is coupled to the rotation of the core represented by N^+ , which is the total angular momentum of the core excluding electron spin [Hund’s case (d), see inset (B) in Fig. 2]. For high n Rydberg states, the external field is dominant; l is decoupled from N^+ , and the angular momenta of both l and N^+ are quantized along the field [decoupled Hund’s case (d), see inset (C) in Fig. 2] [34]. Since the low l (≤ 2) Rydberg electron penetrates the core, it can exchange energy with the core and the core rotation (N^+) can be excited (N^+ -channel interaction). This interaction is negligibly small for nonpenetrating high l (≥ 3) levels [35,36].

Despite these interests, few experimental studies have been conducted for high Rydberg molecules in a high magnetic field because of experimental difficulties, which are described in Ref. [37] in detail. Systematic experiments have so far been conducted by only one research group using nitric oxide (NO) molecules in a field of 0.93 T. The penetrating $7p$ Rydberg state

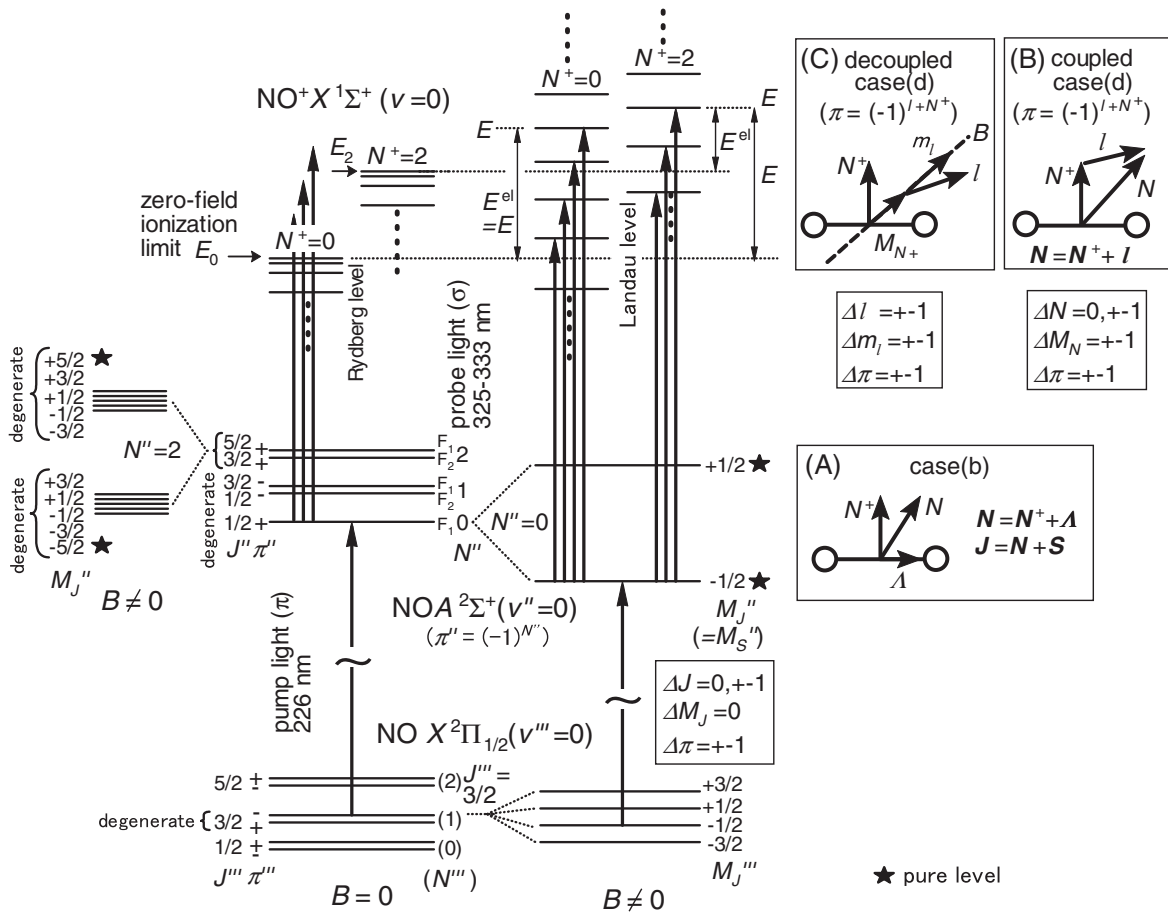


FIG. 2. Schematic energy diagram of the NO molecule. The electronic configuration in its ground state is $(1\sigma)^2(2\sigma)^2(3\sigma)^2(4\sigma)^2(5\sigma)^2(1\pi)^4(2\pi)^1 X^2\Pi$. In a zero field, rotational levels of the ground $X^2\Pi_{1/2}$ and the intermediate $A^2\Sigma^+$ state are shown by successive horizontal lines. Two adjoining lines express degenerate levels. The sign + or - beside the rotational level indicates parity π . Rydberg electronic states converging to the $\text{NO}^+ X^1\Sigma^+(v^+=0, N^+=0)$ or the $\text{NO}^+ X^1\Sigma^+(v^+=0, N^+=2)$ ions are also shown by successive horizontal lines, where E_0 and E_2 are the zero-field ionization limits to each ionic state, respectively. In a magnetic field, the $X^2\Pi_{1/2}(v'''=0, J'''' = 3/2, M_J'''' = -3/2$ to $+3/2)$ and the $A^2\Sigma^+ F_1(v''=0, J'' = 1/2 [N''=0], M_J'' = -1/2$ to $+1/2)$ magnetic sublevels are shown. A star indicates the pure sublevel which contains only F_1 component. Landau levels with the $\text{NO}^+ X^1\Sigma^+(v^+=0, N^+=0)$ core and those with the $\text{NO}^+ X^1\Sigma^+(v^+=0, N^+=2)$ core are shown. For the Landau level of energy E with the $N^+=0$ core, the Rydberg electron's energy is given by $E^{\text{el}} = E$, while that is given by $E^{\text{el}} = E - (E_2 - E_0)$ for the Landau level with the $N^+=2$ core. Two-color double resonance excitation transitions to the Landau levels are shown by vertical arrows. On the left, the $A^2\Sigma^+(v''=0, J'' = 5/2, 3/2 [N''=2], M_J'' = -5/2$ to $+5/2)$ magnetic sublevels are shown. Five sublevels are degenerate. Note that in the present experiment, a single M_J'' sublevel can be selected by exciting from the $N''=0$ level of the intermediate $A^2\Sigma^+$ state. Coupling schemes of the angular momentum corresponding to each electronic state are shown in the insets. Inset (A): Hund's case (b), (B): coupled Hund's case (d), and (C): decoupled Hund's case (d). Selection rules of the transition are shown in a box.

conformed to the intermediate coupling of Hund's cases (b) and (d). The $15p$ and the nonpenetrating $7f$ state conformed to a Hund's case (d). The $15f$ state conformed to a decoupled Hund's case (d). For these states, the N^+ -channel interaction was negligibly small except for the $7p$ state [35,36]. In these energy regions, the diamagnetic term is negligibly small at 0.93 T and the energy structure is completely explained by the linear Zeeman effect. The experiment was extended to the energy region of $n = 35$ – 50 at 0.93 T, where the diamagnetic term is effective. Thus, l -level mixing and n -level mixing were observed, and the energy structure was explained well, including the quadratic Zeeman effect [38]. The energy structure in the -60 to -20 cm^{-1} region observed at 0.93 T was explained successfully by calculating semiclassical wave functions propagating along the closed

classical trajectories [39]. The number of theoretical studies is also few about high Rydberg molecules in a high magnetic field. The energy structure of a high Rydberg hydrogen molecule was calculated by the multichannel quantum defect theory (MQDT) including the paramagnetic term [34] and the diamagnetic term [40]. The energy structure near the zero-field ionization limit was calculated by the combined R matrix and complex coordinate rotation method including the diamagnetic term [41]. The magnetic field-induced structure of the photoabsorption spectrum in the diamagnetic regime was explained theoretically in terms of the inelastic diffractive trajectories of Rydberg electron, which exchanges energy with the molecular core [42–45].

All the above experiments were executed in energy regions below the zero-field ionization limit and at not so high field

(0.93 T). All the calculations were also executed for the Rydberg levels below the limit except for Ref. [41]. Thus, the periodic energy structure formed by the Landau level was not reported. It is interesting to determine whether the coupling between the cyclotron motion of the Rydberg electron and the core rotation [Hund's case (d): $N = l + N^+$] can occur for the positive-energy Landau levels. Here N is the total angular momentum of the molecule excluding electron spin S . Also, it is interesting to determine whether the cyclotron motion penetrates the core and the N^+ -channel interaction can occur in the Landau levels. These subjects can be solved by observing rotational level structures of the Landau level. Nitric oxide molecules are the best for such experiments because they can be considered as one-electron molecules for their high Rydberg states converging to the closed shell $\text{NO}^+ X^1\Sigma^+$ ions, and their simple energy structure has been studied well. In magnetic fields of up to 10 T, our research group excited NO molecules in a gas flow, and the positive-energy Landau levels of molecules were successfully observed [46]. However, their rotational structures were not clearly observed because the transition lines broadened owing to collision-induced line broadening. Because of this result and the fact that the electron cloud of the Landau level spreads to several hundred nanometers from the core, collision-free conditions are necessary.

A new experimental setup having a molecular beam source was built, and molecules under collision-free conditions were thus prepared [37]. In the present study, using this setup, NO molecules are excited to the positive-energy Landau levels by the double-resonance method in a magnetic field of 0–7 T. Measuring the rotational structures of the Landau levels is tried.

II. EXPERIMENT

Figure 3 shows schematically the experimental setup. A magnetic field was generated by a superconducting magnet (10 T). The direction of the field was parallel to the axis ("field axis") of its bore of 100 mm diameter. The field was homogeneous at "field center." A pulsed supersonic beam of

NO molecules with 180 μs pulse duration, 10 Hz repetition rate, and 3 atm stagnation pressure was generated by an orifice of 300 μm diameter and a conical skimmer of 700 μm diameter placed 20 mm downstream. The beam propagated along the field axis in a tube mounted in the bore.

Figure 2 shows a schematic energy diagram of the NO molecules. An excimer laser (wavelength: 308 nm, pulse duration: 25 ns, repetition rate: 10 Hz) pumped Coumarin 440 dye laser. The radiation was frequency doubled into UV radiation (wavelength: 226 nm, bandwidth 0.18 cm^{-1} , pulse energy: $\sim 0.1 \text{ mJ/pulse}$) in a β -barium borate (BBO) crystal. At the field center, the UV radiation was focused and crossed the molecular beam at right angles. The UV radiation was linearly polarized parallel to the magnetic field. It acted as a pump laser to excite the NO molecules from the ground $X^2\Pi_{1/2}(v''' = 0, J''' = 3/2, M_J''' = -1/2)$ rotational sublevel to the intermediate $A^2\Sigma^+ F_1(v'' = 0, J'' = 1/2 [N'' = 0], M_J'' = -1/2)$ sublevel. Here v is the vibrational quantum number; J and M_J denote the quantum numbers associated with the total angular momentum J of the molecule and its projection on the Z axis, respectively; N denotes the quantum number associated with N . The pulse energy of the pump laser was reduced to suppress the two-photon ionization to a negligible level. A probe laser (wavelength: 325–333 nm, bandwidth: 0.18 cm^{-1} , pulse energy: $\sim 0.5 \text{ mJ/pulse}$) was generated by frequency doubling of DCM dye laser pumped by another excimer laser (wavelength: 308 nm, pulse duration: 20 ns, repetition rate: 10 Hz) in a potassium-dihydrogenphosphate (KDP) crystal. The probe laser propagated antiparallel to the pump laser and was linearly polarized perpendicular to the field. The laser pulse was focused on the molecular beam and irradiated it simultaneously with the pump laser. The probe laser further excited the NO $A^2\Sigma^+ F_1(v'' = 0, J'' = 1/2 [N'' = 0], M_J'' = -1/2)$ molecules by the double resonance method to the Landau levels in the energy region above the zero-field ionization limit E_0 to the $\text{NO}^+ X^1\Sigma^+(v^+ = 0, N^+ = 0, M_N^+ = 0)$ ions. Here M_N^+ denotes the quantum number associated with the projection of N^+ on the Z axis.

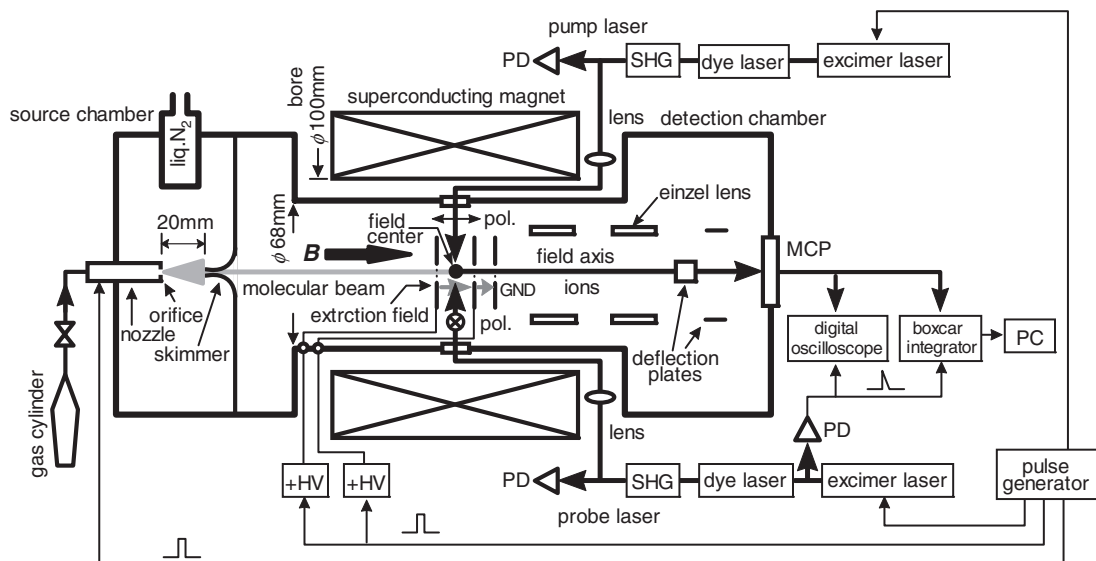


FIG. 3. Experimental setup is schematically shown. Details of the setup are described in Ref. [37].

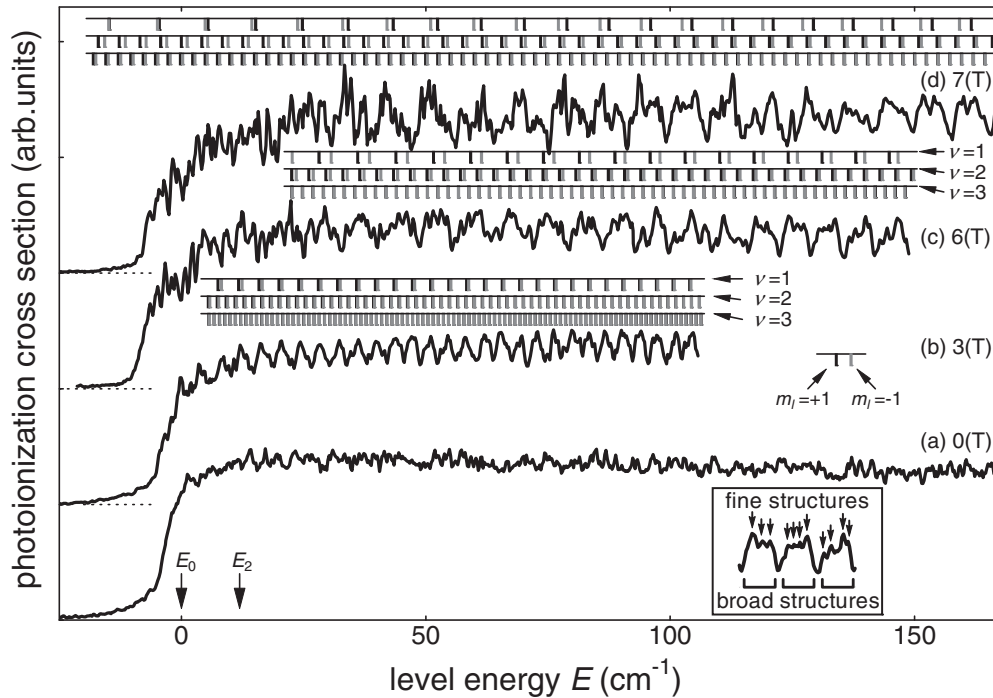


FIG. 4. (a) Photoionization cross section from the intermediate $A^2\Sigma^+F_1(v'' = 0, J'' = 1/2[N'' = 0], M''_j = \pm 1/2)$ sublevels (degenerate) at 0 T. The horizontal axis is the level energy E relative to the zero-field ionization limit E_0 to the $\text{NO}^+ X^1\Sigma^+(v^+ = 0, N^+ = 0)$ ion. The energy E_2 is the zero-field ionization limit to the $\text{NO}^+ X^1\Sigma^+(v^+ = 0, N^+ = 2)$ ion. (b) Photoionization cross section from the intermediate $A^2\Sigma^+F_1(v'' = 0, J'' = 1/2[N'' = 0], M''_j = -1/2)$ sublevel at 3 T. The energy of the $\nu = 1$ –3 Landau levels is shown by the vertical bar. For clarity, bars are not shown in a low energy region, which are shown completely in Fig. 8. Note that the symbol ν denotes the type of the Landau level. Do not confuse it with the vibration of the molecule denoted by v . The illustration in the inset defines the “broad structure” and the “fine structure” in the cross section. (c) Photoionization cross section at 6 T. (d) Photoionization cross section at 7 T.

The symbol “+” on the quantum number indicates that it is associated with the $\text{NO}^+ X^1\Sigma^+$ core. Only Landau levels with $v^+ = 0$ core were produced because of the highly diagonal Franck-Condon factors. Since the electron is not bounded in the direction parallel to the magnetic field in the positive-energy Landau level, the molecules ionized after a while.

A pulsed extraction electric field of 1.4 kV/cm strength and 100 μs duration, which rose 1 μs after laser excitation, was generated between stainless steel plates with openings covered with a high-transmission (>90%) stainless steel mesh. NO^+ ions produced through the Landau levels or by direct ionization were accelerated parallel to the field axis by the extraction field. This parallel extraction prevented the ions from experiencing a Lorentz force. The ions were detected by a microchannel plate (MCP, Hamamatsu, F4655-11X). By the gated time window, a boxcar integrator (Stanford Research Systems SR250) selected the NO^+ ion current (time-of-flight method) and integrated it. The integrated ion current was normalized by the pulse energy of both lasers. Considerable attention was given to the stability of experimental conditions, such as pulse energy of the laser, molecular beam density, and detector efficiency. Details of this setup are given in Ref. [37].

III. RESULTS

A. Experimental results

The ion current, which is proportional to the photoionization cross section from the intermediate $A^2\Sigma^+$ state, was measured as a function of the probe laser’s frequency. Figure 4(a)

shows the result at zero magnetic field. The horizontal axis shows the level energy E relative to the zero-field ionization limit E_0 . The photoionization cross section is negligibly small below the limit E_0 and nearly constant above E_0 . This is contribution of direct ionization. Figure 4(b) shows the cross section in a magnetic field of 3 T. In the positive-energy region, the cross section contains a periodic broad structure with an average energy spacing of 3.7 cm $^{-1}$, which is contribution of the ionization through the Landau level, in addition to the constant term by direct ionization. Figures 4(c) and 4(d) show the cross sections at 6 and 7 T, respectively. The energy spacing of the broad structure increases, in proportion to field strength. These cross sections contain fine structures (0.5–1 cm $^{-1}$ width) that also appear, but are not striking, at 3 T. The measurement was repeated several times to confirm that all fine structures were observed at the same energy.

Figure 5 shows a Fourier transformation of the cross section. The horizontal axis shows time T normalized by the cyclotron period of a free electron $T_C = 2\pi m/eB$. Peaks appear at the same T/T_C in all the fields. The highest peak, marked as $\nu = 1$ at $T/T_C = 0.76$ – 0.79 , is a transformation from the broad structure in the cross section shown in Figs. 4(b)–4(d). The second highest peak ($\nu = 2$) appears at a little less than T_C apart from the $\nu = 1$ peak. The third ($\nu = 3$) and following peaks ($\nu = 4, 5$) appear with spacings equal to T_C , while the latter do not appear clearly except at 6 T. The $\nu = 2, 3, (4, 5)$ peaks are transformations from the fine structures in the cross section.

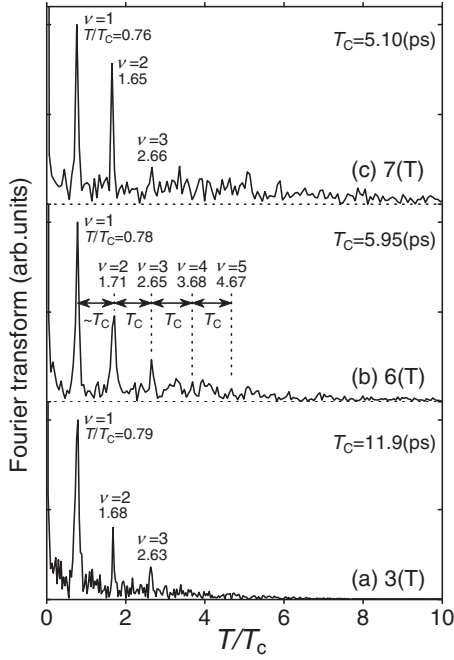


FIG. 5. (a) Fourier transformation of the cross section at 3 T. The horizontal axis is time T normalized by the cyclotron period of a free electron $T_C = 2\pi m/eB$. The value of T/T_C at the peak is shown by the three-digit number. The cross section in the energy region of $E \geq 20 \text{ cm}^{-1}$ in Fig. 4(b) is transformed. (b) Fourier transformation at 6 T. The cross section of $E \geq 40 \text{ cm}^{-1}$ in Fig. 4(c) is transformed. (c) Fourier transformation at 7 T. The cross section of $E \geq 30 \text{ cm}^{-1}$ in Fig. 4(d) is transformed.

These peaks were observed in the Landau levels of atoms and were well explained [18–20,23]. Figure 6 shows classical trajectory calculations of the Rydberg electron explaining these peaks. The insets show the geometries of the calculation, where the Z axis is along the magnetic field. Inset (P) shows the geometry in which two positive $+e$ charges are placed along the X axis at intervals of 0.106 nm on both sides of the origin, which is the equilibrium internuclear distance of the $\text{NO}^+ X^1\Sigma^+$ core. Inset (T) shows a closeup of the core. The valence electron cloud distributed along the internuclear axis is approximated by 11 negative charges $-e/11$ placed at equal intervals (0.0106 nm) along the X axis. Inset (Q) or (R) shows the similar geometry, except that the internuclear axis is along the Y or Z axis, respectively. Instead of rotating the core, these geometries (P)–(R) are adopted for simplicity. Inset (S) shows the atomic case, in which a positive charge $+e$ is placed at the origin. Figures 6(a) and 6(a') show the trajectory at $B = 7 \text{ T}$, calculated for an electron starting near the origin with starting polar angle $\theta_0 = 90^\circ$. The energy of the electron E^{el} is $+100 \text{ cm}^{-1}$, and the Z component of angular-momentum l_Z is $+1 \times \hbar$ (J s) (see the caption of Fig. 6 for the detailed initial condition). The electron returns to the origin and a closed trajectory is formed. Four trajectories with geometries (P)–(S) are overlapped and no difference is found in the recurrence time of the trajectory. Similar calculations are repeated for $B = 3, 6 \text{ T}$. The calculated recurrence times T/T_C are listed in Table I. They are in agreement with the T/T_C of the $\nu = 1$

peaks in Fig. 5 for all the fields. This result indicates that the broad structure in the cross section in Fig. 4 corresponds to the closed classical trajectory in a plane perpendicular to the magnetic field (named as “ $\nu = 1$ trajectory”).

When the electron has a nonzero Z component ($0^\circ < \theta_0 < 90^\circ$) of the starting velocity, solutions are sought for trajectories with an electron starting near the origin and returning there, changing θ_0 as variable for the same E^{el} and l_Z . Figures 6(b), 6(b') or 6(c), 6(c') show the closed trajectory along which the electron rotates around the Z axis two or three times and returns to the origin, respectively. Similar calculations are repeated for $B = 3, 6 \text{ T}$. No difference is found in these results with the four core geometries (P)–(S). The recurrence times of these trajectories are also listed in Table I. All calculated recurrence times T/T_C are in agreement with the T/T_C of the peaks in Fig. 5. This result indicates that the fine structure in the cross section shown in Fig. 4 corresponds to the three-dimensional closed classical trajectory (named as “ $\nu = 2$ trajectory” etc.). For the $\nu = 3$ trajectory, since the second rotation is executed at $Z > 160 \text{ nm}$, the motion is purely cyclotronlike with the period T_C . This is the reason that peaks of $\nu = 3, 4, 5, \dots$ appear with spacings equal to T_C in Fig. 5.

In a classical calculation, the starting angle θ_0 to form a closed trajectory is a continuous function of E^{el} except for the $\nu = 1$ trajectory. The recurrence time T , and thus, the energy spacing between the Landau levels generated by this electron's motion, which is given by $\Delta E^{\text{el}} = h/T$, is a continuous function of E^{el} as well. Here $h = 2\pi\hbar$. The classical calculation gives only the energy spacing but not the absolute value of the level energy [17,47]. Similar trajectory calculations are repeated with several E^{el} and $l_Z = \pm 1 \times \hbar$ (J s) at $B = 3, 6, \text{ and } 7 \text{ T}$. The obtained *scaled* energy spacing given by $\Delta E^{\text{el}}/(2\mu_B B) = T_C/T$ is shown by a mark in Fig. 7. The horizontal axis is the *scaled* energy $E^{\text{el}}/B^{2/3}$. The functional relation between $\Delta E^{\text{el}}/(2\mu_B B)$ and $E^{\text{el}}/B^{2/3}$ is independent of B . This is because the following relations are demonstrated by employing the appropriate scaling transformations for the Hamiltonian including the Coulomb potential energy, the paramagnetic term, and the diamagnetic term. (i) The recurrence time T is proportional to B^{-1} . (ii) Thus, the energy spacing $\Delta E^{\text{el}} (= h/T)$ is proportional to B . (iii) The electron's energy E^{el} is proportional to $B^{2/3}$ [23]. These relations also prove that the recurrence peaks appear at the same T/T_C in all the fields in Fig. 5, and the calculated recurrence time T/T_C is independent of B in Table I. In Fig. 7 the relation between $\Delta E^{\text{el}}/(2\mu_B B)$ and $E^{\text{el}}/B^{2/3}$ is fitted by the fourth or fifth order polynomial function for each field. Results are shown by solid curves in Fig. 7. In the limit of $E^{\text{el}} \rightarrow +\infty$, the energy spacing $\Delta E^{\text{el}}/(2\mu_B B)$ of the “ $\nu = 1$ Landau level” approaches 1. This is because the electron becomes *free* of the Coulomb force, and its motion becomes cyclotron motion of a free electron. As E^{el} decreases to 0 cm^{-1} , the Coulomb force increases, and thus $\Delta E^{\text{el}}/(2\mu_B B)$ increases to 1.5. These results are in agreement with the calculation by the Bohr-Sommerfeld quantization condition applied to atomic Landau levels [15].

In order to determine the energy structure of the Landau levels, the photoionization cross section shown in Fig. 4 is fitted by the function $I(E)$, which is a superposition of the

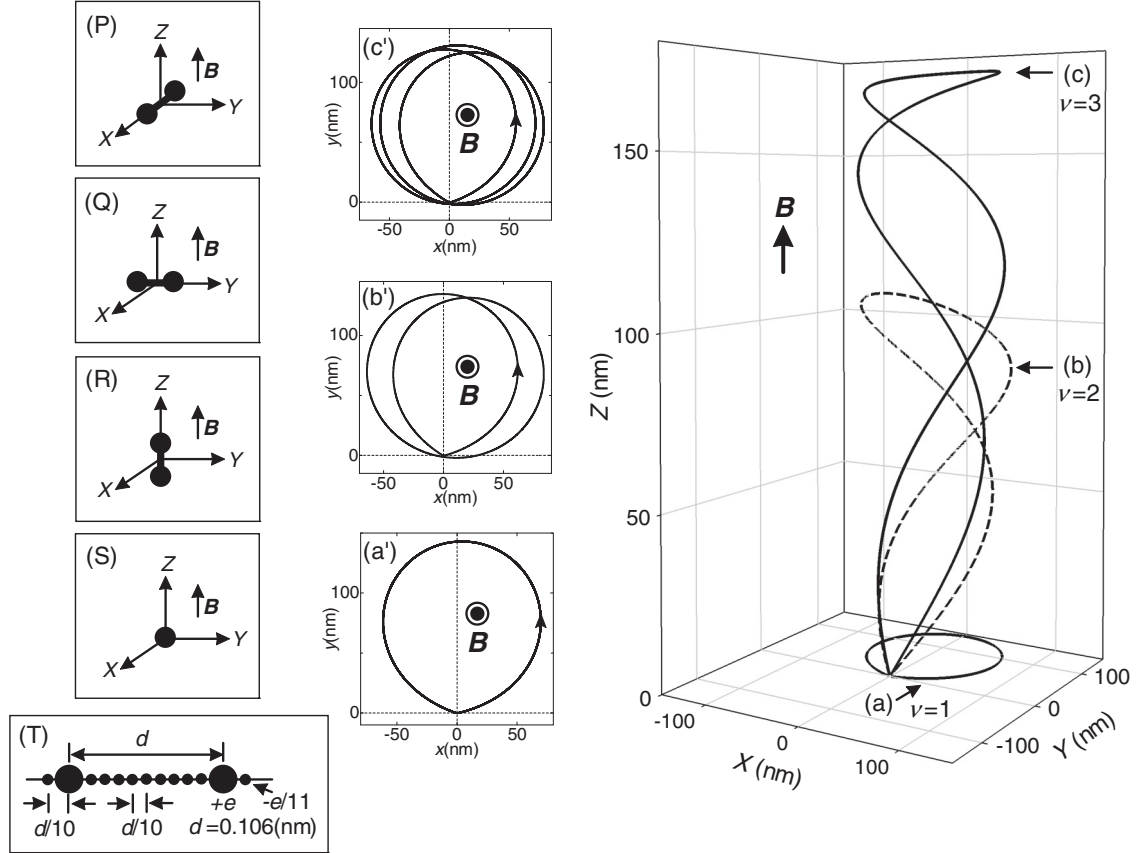


FIG. 6. Classical trajectory calculations of the Rydberg electron having the energy $E^{\text{el}} = +100 \text{ cm}^{-1}$ and the Z component of angular-momentum $l_z = +1 \times \hbar$ (J s) at $B = 7 \text{ T}$, where the Z axis is along the magnetic field. The initial position is the place which is 0.1 nm away from the origin for the atomic core. It is 0.2 nm away from it for the molecular core. Since the starting azimuth angle can be set arbitrarily, the electron starts in the XZ plane in all the calculations. Four trajectories calculated with geometries (P)–(S) are overlapped. (a) $\nu = 1$ trajectory, which is in a plane perpendicular to the magnetic field. (a') Projection of the $\nu = 1$ trajectory onto XY plane. (b) $\nu = 2$ trajectory, along which the electron rotates around the Z axis two times and returns to the origin (three-dimensional trajectory). Note that the electron comes back along the Z axis by the Coulomb force. (b') Projection of the $\nu = 2$ trajectory. (c) $\nu = 3$ trajectory. The electron rotates three times. (c') Projection of the $\nu = 3$ trajectory. (P) Geometry of the molecular core, where the internuclear axis is along the X axis. (Q) Similar to (P), except that the internuclear axis is along the Y axis. (R) Similar to (P), except that the internuclear axis is along the Z axis. (S) Geometry of the atomic core. (T) Closeup of the molecular core.

Gaussian function:

$$I(E) = \left[a_0 + \sum_{\nu=1}^3 \sum_{m_l} a_{\nu} \sum_{N_L} G(E; E_{\nu, m_l, N_L}^{\text{el}} + S_{\nu}, \Gamma_{\nu}) \right] \times [1 - b_1 \exp\{b_2(E - b_3)\}], \quad (1)$$

TABLE I. Recurrence time T/T_C of the closed classical trajectory. For 7 T, the trajectory is shown in Fig. 6. The energy E^{el} of the Rydberg electron is shown in the parentheses. This is nearly the center energy of the cross section that is Fourier transformed (see the caption of Fig. 5). No difference is found in the recurrence time T/T_C with the four core geometries (P)–(S) shown in Fig. 6.

ν	3 T ($E^{\text{el}} = +70 \text{ cm}^{-1}$)	6 T ($E^{\text{el}} = +100 \text{ cm}^{-1}$)	7 T ($E^{\text{el}} = +100 \text{ cm}^{-1}$)
1	0.80	0.79	0.78
2	1.72	1.70	1.69
3	2.71	2.70	2.69
4	3.71	3.70	3.69

where the $\nu = 1-3$ Landau levels are included; m_l denotes the sublevel of the Landau level corresponding to $l_z = \pm 1 \times \hbar$ (J s), and takes +1 and -1; N_L denotes the Landau level of energy $E_{\nu, m_l, N_L}^{\text{el}}$. Note that the zero point of $E_{\nu, m_l, N_L}^{\text{el}}$ is the energy where the energy of the electron E^{el} in the Landau level is zero. Here $G(E; E_{\nu, m_l, N_L}^{\text{el}}, \Gamma_{\nu}) = \exp[-(E - E_{\nu, m_l, N_L}^{\text{el}})^2 / 2\Gamma_{\nu}^2]$ is a Gaussian function with center $E_{\nu, m_l, N_L}^{\text{el}}$ and width Γ_{ν} , excluding normalization factor. The Gaussian function is used for mathematical convenience. Energy shift S_{ν} is introduced to cope with the rotational energy of the core. The coefficient a_0 is a strength of direct ionization and a_{ν} ($\nu = 1-3$) is a strength of ionization through the Landau level. All coefficients a_0-a_3 are assumed to be constant against E . This assumption needs the second term $[1 - b_1 \exp\{b_2(E - b_3)\}]$, which reproduces the rising of the cross section at the limit E_0 . By the fitting, $E_{\nu, m_l, N_L}^{\text{el}}$, a_0-a_3 , S_{ν} , Γ_{ν} , b_1-b_3 are determined under the condition that $E_{\nu, m_l, N_L}^{\text{el}}$ satisfies the relation, which is given by the solid curve in Fig. 7, between energy spacing $\Delta E^{\text{el}} (= |E_{\nu, m_l, N_L}^{\text{el}} - E_{\nu, m_l, N_L-1}^{\text{el}}|)$ and energy E^{el}

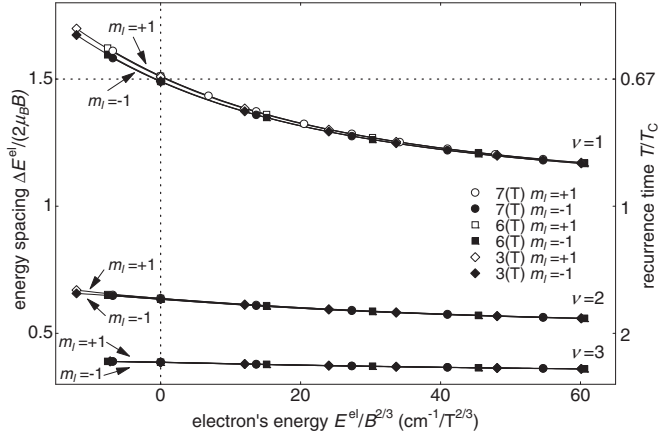


FIG. 7. Marks show the variation in the scaled energy spacing $\Delta E^{\text{el}}/(2\mu_B B)$ of the Landau level, with the scaled energy $E^{\text{el}}/B^{2/3}$ of the Rydberg electron. The symbol $m_l = \pm 1$ denotes the sublevel of the Landau level corresponding to $l_z = \pm 1 \times \hbar$ (J s), respectively. They are obtained by the trajectory calculations. In almost all cases, the initial position for the trajectory calculation is the place which is 0.1 nm away from the origin for the atomic core. It is 0.2 nm away from it for the molecular core. For the $\nu = 3$ levels, the initial position's distance from the origin is larger (≤ 0.5 nm) for low electron's energy E^{el} (i.e., small θ_0). Curves are the fitted results of the relations between $\Delta E^{\text{el}}/(2\mu_B B)$ and $E^{\text{el}}/B^{2/3}$ by the fourth order polynomial function ($\nu = 1$ level) or by the fifth order one ($\nu = 2, 3$ levels). The order of the polynomial function is determined empirically. Three curves for $B = 3, 6, 7$ T are overlapped. Note that $E^{\text{el}} = E$ for the Landau level with the $N^+ = 0$ core, and $E^{\text{el}} = E - (E_2 - E_0)$ for the Landau level with the $N^+ = 2$ core, where E is the level energy of the Landau level.

($= [E_{\nu, m_l, N_L}^{\text{el}} + E_{\nu, m_l, N_L-1}^{\text{el}}]/2$). The number of the independent fitting parameters, which include six energies $E_{\nu, m_l, N_L}^{\text{el}}$, is 19 (see the caption of Fig. 8 for the fitting procedure). Figure 8 shows the resultant $I(E)$ with the measured cross section. All the broad and the fine structures of the cross section are successfully reproduced for all the fields. The determined energy $E_{\nu, m_l, N_L}^{\text{el}} + S_\nu$ of the Landau levels is shown by the vertical bar in Figs. 4 and 8. The determined coefficient a_ν , width Γ_ν , and shift S_ν are listed in Table II. The width Γ_1 is larger than others. This is because a lot of (nearly degenerate) $\nu = 1$ Landau levels lie closely [17] [see Figs. 1(d) and 1(e)]. The shift S_1 is zero, while the averages of S_2 and S_3 are 11.9 and 12.0 cm^{-1} , respectively. The energy spacing between the $X^1\Sigma^+(v^+ = 0, N^+ = 2)$ and the $X^1\Sigma^+(v^+ = 0, N^+ = 0)$

TABLE II. Coefficient a_ν , width Γ_ν , and energy shift S_ν determined by fitting the measured cross section shown in Fig. 4 to Eq. (1). The coefficient a_ν is normalized by a_1 . Trivial parameters a_0 and b_1-b_3 are not listed.

ν	3 T			6 T			7 T		
	a_ν	Γ_ν (cm^{-1})	S_ν (cm^{-1})	a_ν	Γ_ν (cm^{-1})	S_ν (cm^{-1})	a_ν	Γ_ν (cm^{-1})	S_ν (cm^{-1})
1	1.00	0.7	0.0	1.00	0.8	0.0	1.00	1.0	0.0
2	0.30	0.2	11.7	0.47	0.2	11.8	0.70	0.3	12.1
3	0.15	0.2	12.5	0.10	0.2	11.4	0.20	0.3	12.2

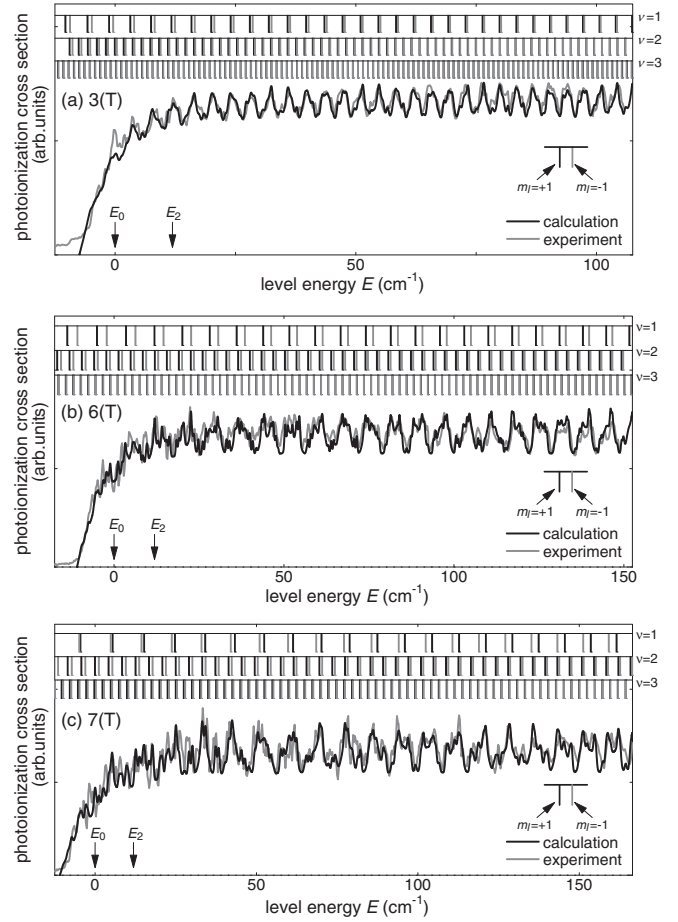


FIG. 8. Black curve shows the calculated photoionization cross section $I(E)$ given by Eq. (1). Gray curve shows the measured cross section that is the same as shown in Fig. 4. The energy of the $\nu = 1-3$ Landau levels is shown by the vertical bar (black: $m_l = +1$, gray: $m_l = -1$). The energy E_0 and E_2 are the zero-field ionization limits to the $\text{NO}^+ X^1\Sigma^+(v^+ = 0, N^+ = 0)$ ion and that to the $\text{NO}^+ X^1\Sigma^+(v^+ = 0, N^+ = 2)$ ion, respectively. The level energy E is related to the electron's energy E^{el} by $E = E^{\text{el}} + (E_2 - E_0)$ for the Landau level with the $N^+ = 2$ core. The shape of the Landau resonance depends on the relative position of the energy of the $m_l = +1$ component of the $\nu = 1$ Landau level, the energy of the $m_l = -1$ component of the $\nu = 1$ level, and the average energy of the $m_l = \pm 1$ components of the $\nu = 2$ level. (a) Result at 3 T. (b) Result at 6 T. (c) Result at 7 T. (*) The fitting method will be explained briefly, assuming that five levels of the $m_l = +1$ component of the $\nu = 1$ Landau level are contained in the photoionization cross section, for simplicity. The electron's energies $E_{\nu, m_l, N_L}^{\text{el}}$ for these levels satisfies $E_{1,+1,1}^{\text{el}} < E_{1,+1,2}^{\text{el}} < E_{1,+1,3}^{\text{el}} < E_{1,+1,4}^{\text{el}} < E_{1,+1,5}^{\text{el}}$. (i) A trial initial value of the highest electron's energy $E_{1,+1,5}^{\text{el}}$ is given. (ii) The energies $E_{1,+1,4}^{\text{el}}$, $E_{1,+1,3}^{\text{el}}$, $E_{1,+1,2}^{\text{el}}$, and $E_{1,+1,1}^{\text{el}}$ are calculated numerically in this order, so that they satisfy the relation which is given by the solid curve in Fig. 7. (iii) Trial initial values of S_1 , a_0-a_1 , Γ_1 , and b_1-b_3 are given. (iv) Equation (1) is calculated using $E_{1,+1,1}^{\text{el}}-E_{1,+1,5}^{\text{el}}$ and S_1 , a_0-a_1 , Γ_1 , b_1-b_3 , and fitted to the measured photoionization cross section shown in Fig. 4 by changing seven parameters of S_1 , a_0-a_1 , Γ_1 , b_1-b_3 . (v) Changing the value of $E_{1,+1,5}^{\text{el}}$, the procedures (ii) and (iv) are repeated and the best values $E_{1,+1,5}^{\text{el}}$, S_1 , a_0-a_1 , Γ_1 , b_1-b_3 are determined. In this stage, best energies $E_{1,+1,1}^{\text{el}}-E_{1,+1,4}^{\text{el}}$ are determined simultaneously. In this example, the number of the independent fitting parameters is 8,

level of the NO^+ core is 11.9 cm^{-1} [48]. Therefore, the core state of the $\nu = 1$ Landau level is $N^+ = 0$ and those of the $\nu = 2, 3$ levels are $N^+ = 2$. Note that the shift S_ν can be determined uniquely because the energy spacing ΔE^{el} is not constant against E^{el} , as shown in Fig. 7. Since the Gaussian functions for the $m_l = \pm 1$ sublevels overlap for the $\nu = 2, 3$ levels, level energy of these sublevels shown in Figs. 4 and 8 has an uncertainty. Therefore, rigorously determined values are the energy of the $m_l = +1$ sublevel of the $\nu = 1$ level, the energy of the $m_l = -1$ sublevel of the $\nu = 1$ level, and the average energy of the adjacent $m_l = \pm 1$ sublevels of the $\nu = 2, 3$ levels. The $\nu = 2, 3$ levels are observed below the limit E_2 because of rotational autoionization (N^+ -channel interaction) through the open $N^+ = 0$ channel [49]. In the future, measurements detecting energy-analyzed electrons will provide another proof of the assignment to the core state (N^+).

The conclusion of this subsection is the following. The broad structure in the cross section in Fig. 4 is formed by the $\nu = 1$ Landau level having the $N^+ = 0$ core and corresponding to the classical trajectory in a plane perpendicular to the magnetic field, while the fine structure is formed by the $\nu = 2, 3$ Landau levels having the $N^+ = 2$ core and corresponding to the three-dimensional classical trajectories. Note that the number ν is used in common to distinguish the peak in the Fourier transformation shown in Fig. 5, the type of the classical trajectory shown in Fig. 6, and the type of the Landau level.

B. Assignment of the Landau levels

The $A^2\Sigma^+$ state of the NO molecules is a Rydberg state, which has s character of 94%, p character of 0.3%, and d character of 5% [50–52]. Since the coupling of S with I is weak in this state, leading to a strong decoupling of S from the internuclear axis toward the external field, the $A^2\Sigma^+$ state conforms to spin-decoupled Hund's case (b) [35]. The basis set is [35,53]

$$|A^2\Sigma^+; S'' M_S'' \eta'' \Lambda'' N'' M_N''\rangle = |S'' M_S''\rangle |\eta'' \Lambda''\rangle |N'' M_N'' \Lambda''\rangle. \quad (2)$$

The first ket represents the electron spin. The second ket represents the radial part of the electronic state. The last ket represents the angular part of molecular rotation. The electronic part of the core and the vibrational part are omitted. Here S and M_S denote the quantum numbers associated with S and S_Z , respectively; Λ and M_N denote the quantum numbers associated with the projection of I on the internuclear axis and the projection of N on the Z axis, respectively. The quantum number η stands for the radial electronic part. Parity of the basis state (2) is given by $\pi'' = (-1)^{N''}$ [35]. In a zero field, all quantum numbers $S'', M_S'', \eta'', \Lambda'', N'', M_N''$ are good

quantum numbers, and M_S'' sublevels are degenerate. In a magnetic field, N'' levels are not mixed by the linear Zeeman effect [54] and the quadratic Zeeman effect is negligibly small for the $A^2\Sigma^+$ state. Therefore, all quantum numbers remain good quantum numbers in a magnetic field. Therefore, selection rules for the transition from the $A^2\Sigma^+ F_1(v'' = 0, J'' = 1/2 [N'' = 0], M_J'' = -1/2)$ sublevel to the Landau level can be evaluated using this basis set. The sublevel of $M_S'' = -1/2$ and $M_N'' = 0$ is selected in the experiment. Parity π'' of the sublevel is $+1$.

When NO molecules were excited from the $A^2\Sigma^+$ state in a zero field or in a low magnetic field below 1 T, transitions to high Rydberg np and nf states were observed [35,36]. The latter transition is due to the strong transition moment to nf state [50,52]. From this result, the small p character in the $A^2\Sigma^+$ state is hereafter ignored. The vibrational selection rule for the transition from the $A^2\Sigma^+$ state to the high Rydberg state is $\Delta v = 0$, because of the highly diagonal Franck-Condon factors caused by the Rydberg character of the $A^2\Sigma^+$ state. In the high Rydberg state of NO molecules, S is decoupled from I , and thus, from the molecular frame [35]. In the following Secs. III C and III D, the energy structure (rotational structure) of the Landau levels is simulated assuming two angular-momentum coupling scheme, i.e., decoupled Hund's case (d) and coupled Hund's case (d). By comparing the simulated energy structure with the structure determined experimentally in Sec. III A and shown in Fig. 8, the angular-momentum coupling scheme of the Landau level will be determined.

C. Assignment by decoupled Hund's case (d)

In this subsection the first model of the angular-momentum coupling for the Landau level will be discussed, where the coupling of I with N^+ is weak or the magnetic field is high enough; thus, I is decoupled from the core rotation N^+ by the field [decoupled Hund's case (d)] [50]. The basis set for the Landau level is [35]

$$|\text{Ryd(D)}; S M_S \eta |l m_l\rangle |N^+ M_N^+ \Lambda^+\rangle = |S M_S\rangle |\eta l\rangle |l m_l\rangle |N^+ M_N^+ \Lambda^+\rangle. \quad (3)$$

The second ket $|\eta l\rangle$ and third ket $|l m_l\rangle$ represent the radial part and angular part of the Rydberg electron's state, respectively. The last ket represents the angular part of the core rotation. The electronic part of the core and the vibrational part are omitted. Here l and m_l denote the quantum numbers associated with I and I_Z , respectively. The symbol “+” on the quantum number indicates that it is associated with the $\text{NO}^+ X^1\Sigma^+$ core. Parity of the basis state (3) is given by $\pi = (-1)^{l+N^+}$ [55].

The matrix element of the transition moment μ'' from the l'' component in the $A^2\Sigma^+$ state to the basis state (3) is [35]

$$\begin{aligned} & \langle A^2\Sigma^+; S'' M_S'' \eta'' \Lambda'' N'' M_N'' | \mu''_{l''} | \text{Ryd(D)}; S M_S \eta |l m_l\rangle |N^+ M_N^+ \Lambda^+\rangle \\ & \propto (-1)^{N''+N^+-\Lambda''-M_N''+m_l} \delta_{S'' S} \delta_{M_S'' M_S} \\ & \quad \times \sqrt{(2l''+1)(2l+1)(2N''+1)(2N^++1)} \\ & \quad \times \begin{pmatrix} l & 1 & l'' \\ 0 & 0 & 0 \end{pmatrix} \begin{pmatrix} l & 1 & l'' \\ -m_l & p & m_l - p \end{pmatrix} \end{aligned}$$

FIG. 8. (Continued) while the number of the fitting parameters determined is 12. In the case shown in this figure, where the $m_l = \pm 1$ components of the $\nu = 1-3$ Landau levels are contained, the number of the independent fitting parameters is 19. They are six $E_{\nu, m_l, N_L^{\text{max}}}^{\text{el}}$ ($\nu = 1, 2, 3; m_l = +1, -1$) and $S_1-S_3, a_0-a_3, \Gamma_1-\Gamma_3, b_1-b_3$, where N_L^{max} is the number of the Landau levels contained.

$$\begin{aligned} & \times \begin{pmatrix} N^+ & l'' & N'' \\ M_N'' - m_l & m_l & -M_N'' \end{pmatrix} \\ & \times \begin{pmatrix} N^+ & l'' & N'' \\ -\Lambda^+ & -\Lambda'' + \Lambda^+ & \Lambda'' \end{pmatrix}, \end{aligned} \quad (4)$$

where l'' denotes the quantum number associated with the electron's orbital angular-momentum l in the $A^2\Sigma^+$ state. Here l'' is not a good quantum number, and l'' can

take 0 or 2 [50–52]. The l'' levels are not mixed by the linear Zeeman effect and the quadratic Zeeman effect is negligibly small for the $A^2\Sigma^+$ state. The symbol p denotes polarization of the photon absorbed during this transition, which is $p = +1$ and $p = -1$ in the present experiment. The selection rules for this transition are $\Delta l = \pm 1, \Delta m_l = \pm 1, \Delta \pi = \pm 1$, and the triangle condition $\Delta(N^+l''N'')$, which is given by $|l'' - N''| \leq N^+ \leq l'' + N''$.

The matrix element of the paramagnetic interaction $H_{\text{para}} = \mu_B B l_Z / \hbar$ in the basis set (3) is

$$\langle \text{Ryd(D)}; S' M_S' \eta' l' m_l' N^+ M_N^+ \Lambda^+ | H_{\text{para}} | \text{Ryd(D)}; S M_S \eta l m_l N^+ M_N^+ \Lambda^+ \rangle = \mu_B B \delta_{S'S'} \delta_{M_S M_S'} \delta_{\eta \eta'} \delta_{l'l'} \delta_{m_l m_l'} \delta_{N^+ N^+} \delta_{M_N^+ M_N^+} \delta_{\Lambda^+ \Lambda^+} m_l. \quad (5)$$

The electron spin part $2\mu_B B S_Z / \hbar$ is omitted because S is decoupled in both $A^2\Sigma^+$ state and high Rydberg state. The matrix element is diagonal in the basis set. No linear Zeeman effect occurs in the $\text{NO}^+ X^1\Sigma^+$ core. Therefore, all quantum numbers remain good quantum numbers. The selection rules for this interaction are $\Delta \eta = 0, \Delta l = 0, \Delta m_l = 0, \Delta N^+ = 0$, and $\Delta M_N^+ = 0$, where, for clarity, only important selection rules are written. The matrix element of the diamagnetic interaction $H_{\text{dia}} = (e^2 B^2 / 8m) r^2 \sin^2 \theta$ is

$$\begin{aligned} & \langle \text{Ryd(D)}; S' M_S' \eta' l' m_l' N^+ M_N^+ \Lambda^+ | H_{\text{dia}} | \text{Ryd(D)}; S M_S \eta l m_l N^+ M_N^+ \Lambda^+ \rangle \\ & = \frac{e^2 B^2}{8m} \delta_{S'S'} \delta_{M_S M_S'} \delta_{N^+ N^+} \delta_{M_N^+ M_N^+} \delta_{\Lambda^+ \Lambda^+} \langle \eta' l' | r^2 | \eta l \rangle \langle l' m_l' | \sin^2 \theta | l m_l \rangle \\ & = \frac{e^2 B^2}{12m} \delta_{S'S'} \delta_{M_S M_S'} \delta_{m_l m_l'} \delta_{N^+ N^+} \delta_{M_N^+ M_N^+} \delta_{\Lambda^+ \Lambda^+} \langle \eta' l' | r^2 | \eta l \rangle \\ & \quad \times \left[\delta_{l'l'} - (-1)^{m_l} \sqrt{(2l+1)(2l'+1)} \begin{pmatrix} l' & 2 & l \\ -m_l & 0 & m_l \end{pmatrix} \begin{pmatrix} l' & 2 & l \\ 0 & 0 & 0 \end{pmatrix} \right]. \end{aligned} \quad (6)$$

The angular part $\langle l' m_l' | \sin^2 \theta | l m_l \rangle$ mixes levels with the selection rules $\Delta l = 0, \pm 2$ and $\Delta m_l = 0$. The radial part $\langle \eta' l' | r^2 | \eta l \rangle$ mixes levels with the selection rules $\Delta \eta = \text{all}$ and $\Delta l = \text{all}$. Therefore, the radial part does not disturb the selection rules induced from the angular part. This was confirmed through many experiments in which the selection rule $\Delta l = 0, \pm 2$ was clearly observed in the quadratic Zeeman effect of Rydberg atoms [2,56]. The quadratic Zeeman effect can be ignored for the core. Therefore, the selection rules for this interaction are $\Delta \eta = \text{all}, \Delta l = 0, \pm 2, \Delta m_l = 0, \Delta N^+ = 0$, and $\Delta M_N^+ = 0$. The total selection rules for the paramagnetic and diamagnetic interactions are $\Delta \eta = \text{all}, \Delta l = 0, \pm 2, \Delta m_l = 0, \Delta N^+ = 0$, and $\Delta M_N^+ = 0$.

The Landau level is formed by the interactions (5) and (6). For the Landau level of atoms, the angular part of the wave function is represented by the spheroidal wave function [12,57,58], which can be expressed by linear combinations of the spherical harmonics $Y_{lm_l}(\theta, \varphi)$ [57]. Thus, the wave function can be expressed by linear combinations of $Y_{lm_l}(\theta, \varphi)$. In this expansion, the coefficient of $Y_{lm_l}(\theta, \varphi)$ is a function of r . Thus, it can be expressed by linear combinations of the radial basis function $\langle r | \eta l \rangle$, which forms a complete basis set. Therefore, the state vector of the atomic Landau level can be expressed by linear combinations of $|\eta l \rangle |l m_l \rangle$. For molecules satisfying decoupled Hund's case (d), the state vector is given by the direct product of the electronic part and the core rotation

part, and the diamagnetic term $H_{\text{dia}} = (e^2 B^2 / 8m) r^2 \sin^2 \theta$ acts on only the electronic part. Thus, its electronic part can be expressed by linear combinations of $|\eta l \rangle |l m_l \rangle$. Therefore, the Landau level is represented by

$$\begin{aligned} & | \text{Land(D)}; N_L S M_S m_l N^+ M_N^+ \Lambda^+ \rangle \\ & = \sum_{\eta} \sum_{l=1,3,5,\dots} c_{\eta,l}^{N_L, N^+, m_l} | S M_S \rangle | \eta l \rangle | l m_l \rangle | N^+ M_N^+ \Lambda^+ \rangle. \end{aligned} \quad (7)$$

The basis states (3) with $l = 1, 3$ are allowed from the $A^2\Sigma^+$ state, according to Eq. (4) and because $l'' = 0, 2$ in the $A^2\Sigma^+$ state. Thus, summation should be taken by η and odd l in Eq. (7), according to the total selection rules of Eqs. (5) and (6). The symbol N_L numbers the Landau level. Strictly speaking, the superscript of the coefficient $c_{\eta,l}^{N_L, N^+, m_l}$ should be $N_L, S, M_S, m_l, N^+, M_N^+, \Lambda^+$. However, according to Eq. (4), $S = 1/2, M_S = -1/2$, and $\Lambda^+ = 0$ are fixed values, and the M_N^+ sublevel is degenerate. Only N_L, N^+, m_l are explicitly shown. Parity of the state (7) is given by $\pi = (-1)^{N^+ + l} = -(-1)^{N^+}$. Figure 1 demonstrates that the spherical basis is unsuitable for expressing the Landau level, because a nearly infinite number of basis states must be included. However, in order to evaluate the transition moment to the Landau level from the intermediate level that is represented appropriately by the spherical basis, the spherical basis is used for the Landau levels.

The Landau levels allowed from the $A^2\Sigma^+F_1(v''=0, J''=1/2 [N''=0], M_J''=-1/2)$ sublevel will be sought according to the selection rules of the transition between the basis set given by Eq. (4) and the state vector of the Landau level given by Eq. (7). The selection rule $\Delta l = \pm 1$ allows the Landau levels of odd l . The selection rule $\Delta\pi = \pm 1$ allows the core states of $N^+ = 0, 2, 4, 6, \dots$. The triangle condition $\Delta(N^+l''N'')$ becomes $N^+ = l''$ and restricts the core states to $N^+ = 0$ or $N^+ = 2$; the Landau levels with the $N^+ = 0$ core are excited using the s character in the $A^2\Sigma^+$ state, whereas those with the $N^+ = 2$ core are excited using its d character. Thus, the selection rule $\Delta m_l = \pm 1$ allows the $m_l = \pm 1$ Landau levels with the $N^+ = 0$ core and the $m_l = -3$ to $+3$ Landau levels with the $N^+ = 2$ core. The Landau levels allowed from the intermediate sublevel are schematically shown in Fig. 9(a). According to the ratio between s and d characters in the $A^2\Sigma^+$ state, transitions to the Landau level with the $N^+ = 0$ core ($v = 1$ level) are expected to be stronger than those to the Landau level with the $N^+ = 2$ core ($v = 2, 3$ levels). This is in agreement with the experimental results shown in Figs. 4 and 5. If the $d \pm 1$ and $d \pm 2$ characters are assumed to be weak in the $A^2\Sigma^+$ state, only $m_l = \pm 1$ Landau levels are allowed for the $N^+ = 2$ core as well, and the energy structure of the Landau levels completely agrees with the experimental results for both core states ($N^+ = 0, 2$).

D. Assignment by coupled Hund's case (d)

In this subsection the second model of the angular-momentum coupling for the Landau level will be discussed, where coupling of l with N^+ holds in a magnetic field and forms the total angular-momentum N [coupled Hund's case (d)]. The basis set for the Landau level is [35]

$$\begin{aligned} & |\text{Ryd(C)}; SM_S\eta l N^+ \Lambda^+ N M_N\rangle \\ & = |SM_S\rangle |\eta l\rangle |(l N^+ \Lambda^+) N M_N\rangle. \end{aligned} \quad (8)$$

The electronic part of the core and the vibrational part are omitted. The ket $|(l N^+ \Lambda^+) N M_N\rangle$ represents the angular part of the molecular rotation, which can be expanded as

$$\begin{aligned} & |(l N^+ \Lambda^+) N M_N\rangle \\ & = (-1)^{N^+ - l - M_N} \sqrt{2N + 1} \sum_{m_l} \sum_{M_N^+} \\ & \times \begin{pmatrix} l & N^+ & N \\ m_l & M_N^+ & -M_N \end{pmatrix} |l m_l\rangle |N^+ M_N^+ \Lambda^+\rangle. \end{aligned} \quad (9)$$

The parity of the basis state (8) is given by $\pi = (-1)^{l+N^+}$ [36,50]. The matrix element of the transition moment $\mu^{l''}$ from the l'' component in the $A^2\Sigma^+$ state to the basis state (8) is [35]

$$\begin{aligned} & \langle A^2\Sigma^+; S'' M_S'' \eta'' l'' N'' M_N'' | \mu_p^{l''} | \text{Ryd(C)}; SM_S\eta l N^+ \Lambda^+ N M_N\rangle \\ & \propto (-1)^{N'' + N^+ + l'' + 1 + M_N - \Lambda''} \delta_{S''S} \delta_{M_S''M_S} \sqrt{(2l'' + 1)(2l + 1)(2N'' + 1)(2N + 1)(2N^+ + 1)} \\ & \times \begin{pmatrix} l & 1 & l'' \\ 0 & 0 & 0 \end{pmatrix} \begin{pmatrix} N & 1 & N'' \\ -M_N & p & M_N'' \end{pmatrix} \begin{pmatrix} N'' & N^+ & l'' \\ \Lambda'' & -\Lambda^+ & \Lambda^+ - \Lambda'' \end{pmatrix} \begin{Bmatrix} N'' & N^+ & l'' \\ l & 1 & N \end{Bmatrix}. \end{aligned} \quad (10)$$

The selection rules for this transition are $\Delta l = \pm 1, \Delta N = 0, \pm 1, \Delta M_N = \pm 1, \Delta\pi = \pm 1$, and $\Delta(N''N^+l'')$.

The matrix element of the paramagnetic interaction $H_{\text{para}} = \mu_B B l_z / \hbar$ in the basis set (8) is

$$\begin{aligned} & \langle \text{Ryd(C)}; S' M_S' \eta' l' N^+ \Lambda^+ N' M_N' | H_{\text{para}} | \text{Ryd(C)}; SM_S\eta l N^+ \Lambda^+ N M_N\rangle \\ & = \mu_B B (-1)^{N^+ + N' + N^+ + l + 1 - M_N} \delta_{S'S} \delta_{M_S'M_S} \delta_{\eta'\eta} \delta_{l'l} \delta_{N^+N^+} \delta_{\Lambda^+\Lambda^+} \\ & \times \sqrt{(2l + 1)(l + 1)l(2N + 1)(2N' + 1)} \begin{pmatrix} N' & 1 & N \\ -M_N' & 0 & M_N \end{pmatrix} \begin{Bmatrix} l & N' & N^+ \\ N & l & 1 \end{Bmatrix}. \end{aligned} \quad (11)$$

The selection rules for this interaction are $\Delta\eta = 0, \Delta l = 0, \Delta N^+ = 0, \Delta N = 0, \pm 1$, and $\Delta M_N = 0$. The matrix element of the diamagnetic interaction $H_{\text{dia}} = (e^2 B^2 / 8m) r^2 \sin^2 \theta$ is

$$\begin{aligned} & \langle \text{Ryd(C)}; S' M_S' \eta' l' N^+ \Lambda^+ N' M_N' | H_{\text{dia}} | \text{Ryd(C)}; SM_S\eta l N^+ \Lambda^+ N M_N\rangle \\ & = \frac{e^2 B^2}{12m} (-1)^{N^+ - M_N} \delta_{S'S} \delta_{M_S'M_S} \delta_{N^+N^+} \delta_{\Lambda^+\Lambda^+} \sqrt{(2l + 1)(2N + 1)(2N' + 1)} \langle \eta' l' | r^2 | \eta l \rangle \\ & \times \left[(-1)^l \delta_{l'l} \begin{pmatrix} N' & 0 & N \\ M_N' & 0 & -M_N \end{pmatrix} \begin{Bmatrix} N' & 0 & N \\ l & N^+ & l' \end{Bmatrix} \right. \\ & \left. - \sqrt{2l' + 1} \begin{pmatrix} l' & 2 & l \\ 0 & 0 & 0 \end{pmatrix} \begin{pmatrix} N' & 2 & N \\ M_N' & 0 & -M_N \end{pmatrix} \begin{Bmatrix} N' & 2 & N \\ l & N^+ & l' \end{Bmatrix} \right]. \end{aligned} \quad (12)$$

The selection rules for this interaction are $\Delta\eta = all, \Delta l = 0, \pm 2, \Delta N^+ = 0, \Delta N = 0, \pm 1, \pm 2$, and $\Delta M_N = 0$. The total selection rules for the paramagnetic and diamagnetic interactions are $\Delta\eta = all, \Delta l = 0, \pm 2, \Delta N^+ = 0, \Delta N = 0, \pm 1, \pm 2$, and $\Delta M_N = 0$.

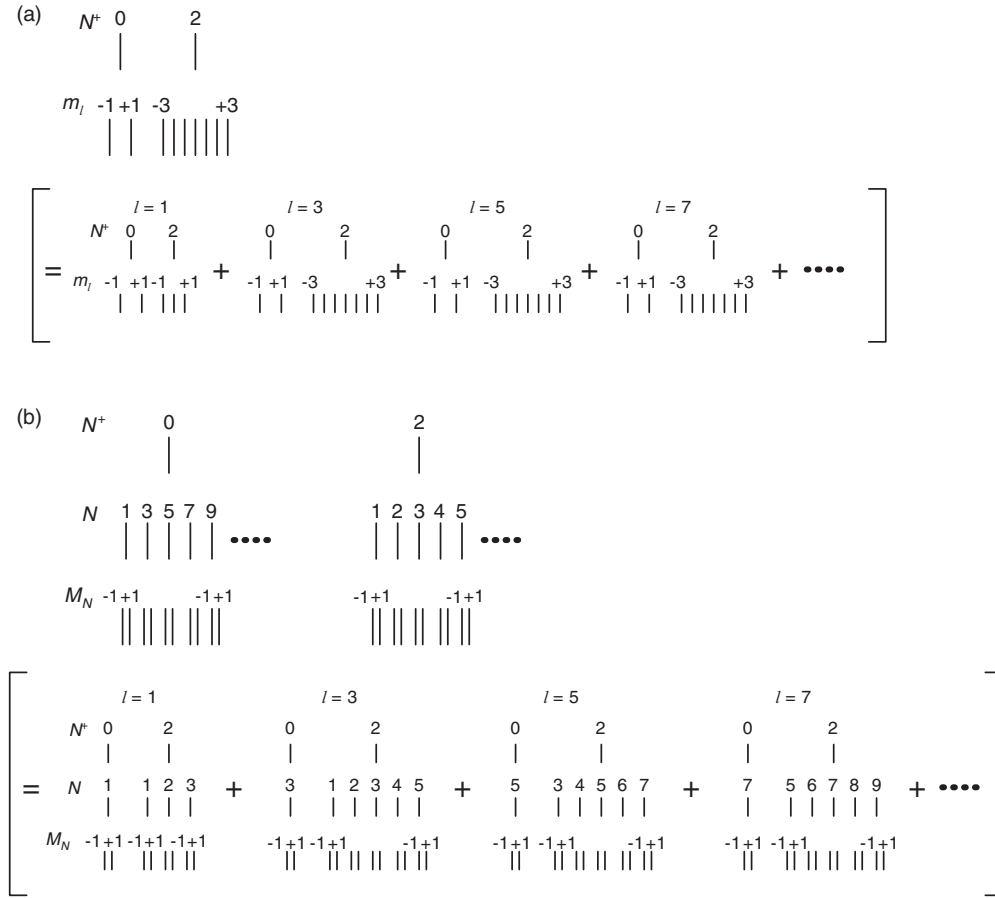


FIG. 9. (a) Schematic energy diagram of the Landau levels allowed from the intermediate $A^2\Sigma^+F_1(v''=0, J''=1/2 [N''=0], M_J''=-1/2)$ sublevel, in case the Landau level conforms to decoupled Hund's case (d). Allowed levels are shown by the vertical bars. In order to understand this energy structure, the allowed levels in case the Landau level consists of one dominant l component and other weak odd l components are shown in the parentheses. The dominant l component is shown as " $l=1$," etc. at the top of each structure and acts as the structure's name. These levels may be the Rydberg levels in a negative energy region ($E < 0$) rather than Landau levels [see Fig. 1(b)]. The $l=1, 3, 5, 7, \dots$ structures are not degenerate at $E < 0$. As the level energy E becomes positive, the $l=1, 3, 5, 7, \dots$ structures become degenerate [see Figs. 1(d) and 1(e)], and note this means the Landau levels become degenerate and does not mean the l levels become degenerate., and then, the energy structure shown at the top is formed. (b) Similar energy diagram in case the Landau level conforms to coupled Hund's case (d). The symbol " \dots " beside the N levels means that the N levels continue as long as those levels have the $N=1$ component (character).

The state vector of the Landau level is represented by

$$|\text{Land}(C); N_L S M_S N^+ \Lambda^+ M_N\rangle = \sum_{\eta} \sum_{l=1,3,5,\dots} \sum_{N=|l-N^+|}^{l+N^+} c_{\eta,l,N}^{N_L, N^+, M_N} |S M_S\rangle |\eta l\rangle |(l N^+ \Lambda^+) N M_N\rangle. \quad (13)$$

The basis states (8) with $l=1, 3$ are allowed from the $A^2\Sigma^+$ state, according to Eq. (10) and because $l''=0, 2$ in the $A^2\Sigma^+$ state. Thus, summation should be taken by N, η , and odd l in Eq. (13), according to the total selection rules from Eqs. (11) and (12). This indicates that all N levels and all odd l levels are mixed. Only significant quantum numbers are shown explicitly as the superscript of $c_{\eta,l,N}^{N_L, N^+, M_N}$ among $N_L, S, M_S, N^+, \Lambda^+, M_N$, because of the similar reason mentioned for Eq. (7) and according to Eq. (10). Parity of the state (13) is given by $\pi = (-1)^{N^++l} = -(-1)^{N^+}$.

The Landau levels allowed from the intermediate sublevel will be sought according to the selection rules of the transition

between the basis set given by Eq. (10) and the state vector of the Landau level given by Eq. (13). The selection rule $\Delta l = \pm 1$ allows the Landau levels of odd l . The selection rule $\Delta \pi = \pm 1$ allows the core states of $N^+ = 0, 2, 4, 6, \dots$. The triangle condition $\Delta(N^+ l'' N'')$ becomes $N^+ = l''$ for $N'' = 0$, and restricts the core states to $N^+ = 0, 2$. The selection rule $\Delta N = 0, \pm 1$ allows the $N = 0, 1$ components of the Landau levels. However, since no $N = 0$ component is formed from an odd l component and even N^+ level, only the Landau levels having the $N = 1$ component (character) are allowed. All (mixed) N levels have the $N = 1$ component according to Eq. (13), or originally because of the selection rules for

the total Zeeman interaction $\Delta N = 0, \pm 1, \pm 2$. Therefore, all (mixed) N levels are allowed. The selection rule $\Delta M_N = \pm 1$ allows the $M_N = +1$ and the $M_N = -1$ Landau level. The Landau levels allowed from the intermediate sublevel are schematically shown in Fig. 9(b). In this way, although the Landau levels are excited from the $N'' = 0$ level of the $A^2\Sigma^+$ state, many N levels can be excited, which is necessary for determining the N structure of the Landau level. For the present energy region, the energy separation between the adjacent N levels is estimated to be about 1.2 cm^{-1} , which is scaled from the energy separations between them in the Rydberg states by using the electron radius in the classical trajectory [35,36,50,59]. Including this N structure in Eq. (1), the shape of the cross section calculated is not in agreement with the experimental result shown in Fig. 4. Therefore, the coupled Hund's case (d) model is rejected.

E. Conclusion of the assignment

From the discussions in Secs. III C and III D, it is concluded that in a field of 3–7 T, the Landau level conforms to decoupled Hund's case (d). The $\nu = 1$ Landau level (core: $N^+ = 0$) is excited using the s character in the $A^2\Sigma^+$ state, while the $\nu = 2, 3$ Landau levels (core: $N^+ = 2$) are excited using the d character.

Core-excited ($N^+ = 2$) Landau levels are observed, as expected according to the selection rule $N^+ = l''$. However, from the present analysis only, it cannot be concluded that the $N^+ = 2$ core is generated through the N^+ -channel interaction in the Landau levels having a penetrating p character because the intermediate $A^2\Sigma^+ F_1(v'' = 0, J'' = 1/2 [N'' = 0], M''_j = -1/2)$ sublevel may have the $N^{+''} = 2$ character in addition to the $N^{+''} = 0$ character. In the present analysis, only paramagnetic and diamagnetic interactions are included in the interaction Hamiltonian. If the molecular core anisotropy is included rigorously in it, the summation should be taken by N^+ and m_l , in addition to η and l in Eq. (7) [38] and the coefficient c can be determined by diagonalizing the total Hamiltonian. Then, the N^+ -channel interaction in the Landau levels will be analyzed rigorously in the future. The assignment shown in Fig. 8 indicates that m_l mixing can be neglected for the $\nu = 1$ Landau levels in 3–7 T. A rigorous judgment is impossible about the $\nu = 2, 3$ levels because of the energy resolution of the laser.

Quantum defect theory (QDT) was developed for analyzing the energy structure and dynamics of atom's Rydberg states. For atoms, the Rydberg electron suffers an anisotropic interaction resulting from electron correlation near the core. However, in a region far from the core, it feels only isotropic Coulomb potential energy, and thus, the radial wave function is expressed by the linear combination of the regular [$f(\xi, r)$] and irregular [$g(\xi, r)$] Coulomb functions, where ξ is the effective quantum number (usually written as ν). The phase of the Coulomb function's coefficient is the quantum defect $\mu (= n - \xi)$, which depends on the interaction near the core. For molecules, the core anisotropy also causes the anisotropic interaction near the core. Nevertheless, in a region far from the core, the Rydberg electron's condition is similar to that of atoms. Thus, the electronic radial wave function is expressed by the Coulomb functions in there. In a high magnetic field,

however, the Rydberg electron feels the diamagnetic term in addition to the Coulomb potential energy in a region far from the core. Thus, the electronic radial part of the wave function cannot be expressed by the linear combination of the regular and irregular Coulomb functions. Basis functions for the electronic part can be obtained by diagonalizing the Hamiltonian including the Coulomb potential energy and the diamagnetic term, over a set of Sturmian functions (radial part) and the spherical harmonics (angular part) [8,40].

According to the procedure by multichannel quantum defect theory (MQDT) applied to the molecular Rydberg states [34,40,60], wave functions for the molecular Landau levels are derived dividing the region into three as follows. Here the electron spin part and the core radial part (core vibration) are ignored. (i) In the inner region, where l of the Rydberg electron is coupled to the internuclear axis [Hund's case (b)], the Rydberg series are classified by l and Λ , and have the quantum defect $\mu_{l\Lambda}$. The difference between $\mu_{l\Lambda}$ of different Λ indicates the molecular core anisotropy. The quantum defect $\mu_{l\Lambda}$ is nearly zero for high l states. Considering the N -level mixing (if exist) by the paramagnetic term and the l uncoupling, the total wave function is given by $\Psi_I = \sum_{l\Lambda N} A_{l\Lambda N} [f(\xi, r) \cos \pi \mu_{l\Lambda} - g(\xi, r) \sin \pi \mu_{l\Lambda}] |N M_N \Lambda\rangle$, where the total angular part $|N M_N \Lambda\rangle$ is made of the Hund's case (b) coupling between the electronic angular part and the core angular part (core rotation). The unknown coefficients $A_{l\Lambda N}$ are determined later. (ii) In the outer region, where l is decoupled from N^+ by the magnetic field [decoupled Hund's case (d)] but the diamagnetic term is negligibly smaller than the paramagnetic term, the Rydberg series converge to the channels classified by N^+ and m_l . The wave function is obtained by the frame transformation of Ψ_I from case (b) to decoupled case (d). The interaction between N^+, m_l channels resulting from the molecular core anisotropy is brought in, through the quantum defect $\mu_{l\Lambda}$ defined in region (i). Considering the channel interaction, the total wave function is given by $\Psi_{II} = \sum_{N^+ m_l} [C_{N^+ m_l} f(\xi_{N^+ m_l}, r) - D_{N^+ m_l} g(\xi_{N^+ m_l}, r)] |l m_l\rangle |N^+ M_N^+ \Lambda^+\rangle$, where $|l m_l\rangle$ and $|N^+ M_N^+ \Lambda^+\rangle$ are the electronic angular part and the core angular part, respectively. The coefficients $C_{N^+ m_l}$ and $D_{N^+ m_l}$ in the electronic radial part are functions of the frame-transformation matrix, the quantum defects $\mu_{l\Lambda}$, and the unknown coefficient $A_{l\Lambda N}$. Since the diamagnetic term is negligibly smaller than the paramagnetic term in regions (i) and (ii), the Coulomb functions can be used as the electronic radial wave function. (iii) In the outermost region, the Rydberg electron feels the Coulomb potential energy and the diamagnetic term. As outlined in the previous paragraph, the basis function is given by $\psi_{KN^+ m_l} = \sum_{nl} F_{Knl m_l} S_{nl}^\zeta(r) |l m_l\rangle |N^+ M_N^+ \Lambda^+\rangle$, where $S_{nl}^\zeta(r)$ is the Sturmian function (electronic radial part). The integer K numbers the basis functions. The coefficient $F_{Knl m_l}$ is determined by diagonalizing the Hamiltonian including the Coulomb potential energy and the diamagnetic term. Note that the paramagnetic term is negligibly smaller than the diamagnetic term and can be disregarded. Considering the anisotropic interaction in region (i), the total wave function is given by $\Psi_{III} = \sum_{KN^+ m_l} \alpha_{KN^+ m_l} \psi_{KN^+ m_l}$, where $\alpha_{KN^+ m_l}$ are unknown coefficients. By matching the total wave function Ψ_{III} with Ψ_{II} at the boundary between regions (ii) and

(iii) using R -matrix procedure [8], the unknown coefficients $A_{l\Delta N}$ and α_{KN+m_l} are determined. In this way, all the wave functions $\Psi_I, \Psi_{II}, \Psi_{III}$ are determined. The periodic energy structure corresponding to the Landau levels will be obtained by calculating the level-energy dependence of the transition probability from the intermediate level to the state represented by the wave functions $\Psi_I, \Psi_{II}, \Psi_{III}$.

Though the wave functions were calculated successfully by this method using Sturmian functions for the Rydberg states below $n \sim 30$ of both atoms [8] and molecules [40], the calculation will be difficult for the positive energy Landau levels because Sturmian functions with nearly infinite n and l need to be included as basis functions. Thus, the merit of MQDT that the summation over n is implicitly preformed is lost. Therefore, the labor of the calculation is comparable to diagonalizing the Hamiltonian, which includes the molecular core anisotropy as the multipole moments of the core charge distribution, over the basis function Eq. (7).

IV. DISCUSSION

The state vector Eq. (7) of the Landau level [i.e., decoupled Hund's case (d)] indicates that the angular part of the electronic wave function can be expanded in terms of the spherical harmonics $Y_{lm_l}(\theta, \varphi)$, where θ and φ are polar and azimuth angles, respectively. Therefore, the partial wave expansion can be applied to explain the starting polar angles of the classical trajectories corresponding to the $\nu = 1-3$ Landau levels, as Main *et al.* has applied it to the atomic Landau levels [19].

Since the $\nu = 1$ Landau level is excited using the s character in the $A^2\Sigma^+$ state, the dominant partial wave is $Y_{1\pm 1}(\theta, \varphi)$. The spherical harmonics $Y_{1\pm 1}(\theta, \varphi)$ have a maximum amplitude at $\theta = 90^\circ$, which is the starting polar angle of the $\nu = 1$ classical trajectory shown in Fig. 6(a). The amplitude of $Y_{1\pm 1}(\theta, \varphi)$ decreases to zero, as θ decreases from 90° to 0° passing through the starting polar angles $\theta_0 = 53^\circ$ and 40° of the $\nu = 2, 3$ trajectories, respectively [see Figs. 6(b) and 6(c)]. This angular distribution is in agreement with the fact that the $\nu = 1$ level corresponds to the classical trajectory in a plane perpendicular to the magnetic field [Fig. 6(a)]. In many experiments with atoms, they were excited from the s state by the light circularly polarized along the magnetic field, and the $\nu = 1$ Landau level was observed [9, 12, 14]. These results are similarly explained well by the above-mentioned angular distribution. For the $\nu = 2, 3$ levels, the dominant partial wave is $Y_{3\pm 1}(\theta, \varphi)$ according to the assignment shown in Fig. 8, because the $\nu = 2, 3$ levels are excited using the d character in the $A^2\Sigma^+$ state and because the amplitude of the f wave is one order larger than that of p wave [61]. However, $Y_{3\pm 1}(\theta, \varphi)$ has a maximum amplitude at $\theta = 31.1^\circ$. A contribution of the $Y_{3\pm 2}(\theta, \varphi)$ partial wave, which has a maximum amplitude at $\theta = 54.7^\circ$, cannot be neglected. This argument indicates that the d_0 and $d \pm 1$ characters are dominant over the $d \pm 2$ character in the $A^2\Sigma^+$ state, and $m_l = 0, \pm 1, \pm 2$ Landau levels should be observed. However, these levels cannot be resolved clearly by the limit of the laser's energy resolution. High resolution experiment using cw laser may solve this problem in the future.

In the present experiment the Landau levels are excited from the intermediate state of *molecules*, which has both the

atomic s and d characters. Thus, two (or three) dominant partial waves are generated simultaneously, and the total wave has a large amplitude at both the starting angles of the $\nu = 1$ and the $\nu = 2$ trajectory. Therefore, the $\nu = 1$ and the $\nu = 2$ Landau levels are observed simultaneously in a single measurement. Note that the $\nu = 1$ and the $\nu = 2$ Landau levels are observed in separate measurements in *atoms*, where polarization of the light or a magnetic sublevel of the lower state is different [18, 19, 21].

In the present experiment the Landau levels are excited from the $N'' = 0$ level of the intermediate $A^2\Sigma^+$ state, and thus, the triangle condition $\Delta(N^+l''N'')$ in Eq. (4) or (10) becomes a simple form of $N^+ = l''$. This equation relates the core state (N^+) to the dominant partial wave. Therefore, the type of the Landau level (ν) corresponds uniquely with the core state N^+ . In addition, the $N'' = 0$ level is selected by other following reasons: (i) Overlap of the pump $X^2\Pi_{1/2}-A^2\Sigma^+$ rotational transitions is avoided most easily than pumping other N'' levels [37]. (ii) Population is largest among the N'' levels [37]. (iii) Overlap of the M_J'' sublevel is avoided as explained in Fig. 2. Since the $\text{NO}^+ X^1\Sigma^+$ core exhibits no linear Zeeman effect and negligibly small quadratic Zeeman effect, the NO molecule has no M_{N^+} splitting of the ionization limit. All these conditions make it possible to excite the Landau level having a simplest energy structure to determine successfully the angular-momentum coupling.

In our previous experiment using NO molecules in a gas flow, even the $\nu = 1$ Landau level was not observed below 6 T, and no $\nu \geq 2$ levels were observed at 0–10 T [46]. The classical trajectory calculation of the electron having energy of $E^{\text{el}} = +100 \text{ cm}^{-1}$, for example, shows that the maximum radius of the electron in the $\nu = 1$ Landau level is 163 nm at 6 T. As the field B decreases, the maximum radius increases depending on $B^{-2/3}$ for the level of the same scaled energy. On the other hand, the maximum radii of the $\nu = 2$ and $\nu = 3$ trajectories are 174 and 244 nm at 6 T, respectively. (Note trajectories shown in Fig. 6 are calculated at 7 T.) If ~ 170 nm is assumed to be the threshold radius for the molecules to survive in the gas flow of the previous experiment, it is explained reasonably that no $\nu \geq 2$ Landau levels were observed. In the present experiment, by the collision-free conditions, Landau levels are observed clearly even at 3 T, and the $\nu = 2, 3$ Landau levels, which have larger radii than the $\nu = 1$ level, are also observed successfully at 3–7 T. In addition, collision-induced line broadening is reduced by the collision-free conditions, and thus, the fine structure of the Landau resonance becomes clear. Figure 5 shows that the strength of the $\nu = 2, 3$ levels increases with the magnetic field. This may result from not only the change in the transition probability, which is induced by the field-dependent change in the relative strength of the l character in the Landau level, but also the reduction in the classical trajectory's radius as the field increases. As the level energy E increases, the radius of the electron in the Landau level becomes larger. Therefore, as E increases higher above the present range shown in Fig. 4, first, the amplitude of the fine structure will decrease in the photoionization cross section; then, the amplitude of the broad structure will decrease; and finally, the plateau will decrease quite slowly.

High Rydberg molecules are sensitive to a stray electric field F . The interaction energy between the field F and the

molecule is $e\mathbf{r} \cdot \mathbf{F}$, where \mathbf{r} is the Rydberg electron's radius. The maximum electron radii of the classical trajectories shown in Fig. 6, where $E^{\text{el}} = +100 \text{ cm}^{-1}$ and $B = 7 \text{ T}$, are 143 nm ($\nu = 1$), 154 nm ($\nu = 2$) and 219 nm ($\nu = 3$), respectively. Thus, for a stray electric field of 100 mV/cm, the maximum interaction energies are estimated to be 0.011 cm^{-1} ($\nu = 1$), 0.012 cm^{-1} ($\nu = 2$), and 0.018 cm^{-1} ($\nu = 3$), respectively. On the other hand, the observed energy spacings between the Landau levels around $E^{\text{el}} = +100 \text{ cm}^{-1}$ are 8.4 cm^{-1} ($\nu = 1$), 3.9 cm^{-1} ($\nu = 2$), and 2.4 cm^{-1} ($\nu = 3$), respectively at 7 T, which are 2 orders larger than the interaction energies. Therefore, the stray electric field needs to be reduced to 100 mV/cm.

When twice the energy difference between the core rotational states (N^+) is the same as an integral ($=k$) multiple of the energy spacing between the Landau levels (named "stroboscopic condition"), the Rydberg electron sees the internuclear axis in the same direction whenever it approaches the core. This means that Λ is a good quantum number and the coupling is Hund's case (b). This periodic return to Hund's case (b) is called stroboscopic effect [62,63]. A magnetic field of 3–7 T cannot decouple the angular-momentum \mathbf{l} from the *internuclear axis* [54]. Therefore, when the stroboscopic condition is satisfied, if the Landau levels conform to Hund's case (b), additional energy structure, which is similar to the N structure in coupled Hund's case (d) shown in Fig. 9(b), may be included in the photoionization cross section. If \mathbf{l} needs

to be decoupled from the internuclear axis in order for the Rydberg electron to carry out cyclotron motion around the core, Landau levels may not be observed. At 6 T, the observed photoionization cross section shown in Fig. 4(c) or 8(b) contains the $\nu = 1$ Landau level ($E \sim 28 \text{ cm}^{-1}$) which satisfies the stroboscopic condition ($k = 3$) between the $N^+ = 0$ and the $N^+ = 2$ cores. However, no significant change is observed in the shape of the structure in the cross section. Systematic exploration is necessary in the future.

In conclusion, in a magnetic field of 0–7 T, the molecular Landau levels ($\nu = 2, 3$) having the *excited* $N^+ = 2$ cores and corresponding to the three-dimensional classical trajectories are observed, in addition to the Landau level ($\nu = 1$) having the $N^+ = 0$ core and corresponding to the classical trajectory in a plane perpendicular to the field. The selection rule of the excitation ($N^+ = l''$) relates the core state (N^+) to the dominant partial wave. Its angular distribution explains well the starting polar angles of the $\nu = 1-3$ classical trajectories. The electron's orbital angular-momentum \mathbf{l} is decoupled from the core rotation N^+ in the Landau levels.

ACKNOWLEDGMENTS

This study was partly supported by a Grant-in-Aid for Scientific Research from the Japan Society for the Promotion of Science (JSPS) (Grants No. 18540396 and No. 22540413).

-
- [1] F. A. Jenkins and E. Segre, *Phys. Rev.* **55**, 52 (1939).
 - [2] M. L. Zimmerman, J. C. Castro, and D. Kleppner, *Phys. Rev. Lett.* **40**, 1083 (1978).
 - [3] R. J. Fonck, F. L. Roesler, D. H. Tracy, K. T. Lu, F. S. Tomkins, and W. R. S. Garton, *Phys. Rev. Lett.* **39**, 1513 (1977).
 - [4] A. R. Edmonds, *J. Phys. B* **6**, 1603 (1973).
 - [5] C. W. Clark and K. T. Taylor, *J. Phys. B* **13**, L737 (1980).
 - [6] C. W. Clark and K. T. Taylor, *J. Phys. B* **15**, 1175 (1982).
 - [7] G. Hose, H. S. Taylor, and D. Richards, *J. Phys. B* **18**, 51 (1985).
 - [8] P. F. O'Mahony and K. T. Taylor, *Phys. Rev. Lett.* **57**, 2931 (1986).
 - [9] W. R. S. Garton and F. S. Tomkins, *Astrophys. J.* **158**, 839 (1969).
 - [10] R. J. Fonck, D. H. Tracy, D. C. Wright, and F. S. Tomkins, *Phys. Rev. Lett.* **40**, 1366 (1978).
 - [11] K. T. Lu, F. S. Tomkins, H. M. Crosswhite, and H. Crosswhite, *Phys. Rev. Lett.* **41**, 1034 (1978).
 - [12] K. T. Lu, F. S. Tomkins, and W. R. S. Garton, *Proc. R. Soc. London Sect. A* **362**, 421 (1978).
 - [13] R. J. Fonck, F. L. Roesler, D. H. Tracy, and F. S. Tomkins, *Phys. Rev. A* **21**, 861 (1980).
 - [14] W. R. S. Garton, F. S. Tomkins, and H. M. Crosswhite, *Proc. R. Soc. London Sect. A* **373**, 189 (1980).
 - [15] A. F. Starace, *J. Phys. B* **6**, 585 (1973).
 - [16] W. P. Reinhardt, *J. Phys. B* **16**, L635 (1983).
 - [17] D. Wintgen and H. Friedrich, *Phys. Rev. A* **36**, 131 (1987).
 - [18] A. Holle, G. Wiebusch, J. Main, B. Hager, H. Rottke, and K. H. Welge, *Phys. Rev. Lett.* **56**, 2594 (1986).
 - [19] J. Main, G. Wiebusch, A. Holle, and K. H. Welge, *Phys. Rev. Lett.* **57**, 2789 (1986).
 - [20] M. A. Al-Laihy, P. F. O'Mahony, and K. T. Taylor, *J. Phys. B* **19**, L773 (1986).
 - [21] J. Neukammer, H. Rinneberg, K. Vietzke, A. König, H. Hieronymus, M. Kohl, H.-J. Grabka, and G. Wunner, *Phys. Rev. Lett.* **59**, 2947 (1987).
 - [22] M. A. Al-Laihy and C. M. Farmer, *J. Phys. B* **20**, L747 (1987).
 - [23] J. Main, A. Holle, G. Wiebusch, and K. H. Welge, *Z. Phys. D* **6**, 295 (1987).
 - [24] A. Holle, J. Main, G. Wiebusch, H. Rottke, and K. H. Welge, *Phys. Rev. Lett.* **61**, 161 (1988).
 - [25] M. L. Du and J. B. Delos, *Phys. Rev. A* **38**, 1896 (1988).
 - [26] P. F. O'Mahony, *Phys. Rev. Lett.* **63**, 2653 (1989).
 - [27] D. Wintgen and H. Friedrich, *Phys. Rev. Lett.* **57**, 571 (1986).
 - [28] Q. Wang and C. H. Greene, *Phys. Rev. A* **40**, 742 (1989).
 - [29] R. H. Garstang, *Rep. Prog. Phys.* **40**, 105 (1977).
 - [30] H. J. Beyer and H. Kleinpoppen (eds.), *Progress in Atomic Spectroscopy, Part C* (Plenum, New York, 1984), Chaps. 6 and 7.
 - [31] T. F. Gallagher, *Rydberg Atoms* (Cambridge University Press, Cambridge, 1994).
 - [32] Edited by G. W. Series, *The Spectrum of Atomic Hydrogen Advances* (World Scientific, Singapore, 1988), Chap. 7.
 - [33] H. Ruder, G. Wunner, H. Herold, and F. Geyer, *Atoms in Strong Magnetic Fields* (Springer, New York, 1994).
 - [34] T. S. Monteiro and K. T. Taylor, *J. Phys. B* **22**, L191 (1989).
 - [35] S. Guizard, N. Shafizadeh, M. Horani, and D. Gauyacq, *J. Chem. Phys.* **94**, 7046 (1991).

- [36] M. Raoult, S. Guizard, and D. Gauyacq, *J. Chem. Phys.* **95**, 8853 (1991).
- [37] Y. Kimura and K. Takazawa, *Rev. Sci. Instrum.* **82**, 013108 (2011).
- [38] M. Raoult, S. Guizard, D. Gauyacq, and A. Matzkin, *J. Phys. B* **38**, S171 (2005).
- [39] A. Matzkin, M. Raoult, and D. Gauyacq, *Phys. Rev. A* **68**, 061401 (2003).
- [40] T. S. Monteiro and K. T. Taylor, *J. Phys. B* **23**, 427 (1990).
- [41] X. H. He, K. T. Taylor, and T. S. Monteiro, *J. Phys. B* **28**, 2621 (1995).
- [42] A. Matzkin and T. S. Monteiro, *Phys. Rev. Lett.* **87**, 143002 (2001).
- [43] A. Matzkin, P. A. Dando, and T. S. Monteiro, *Phys. Rev. A* **66**, 013410 (2002).
- [44] A. Matzkin, P. A. Dando, and T. S. Monteiro, *Phys. Rev. A* **67**, 023402 (2003).
- [45] D. Wang, Q. Xu, C. Yang, M. Wang, and X. Ma, *J. Chem. Phys.* **129**, 104310 (2008).
- [46] K. Takazawa and H. Abe, *J. Chem. Phys.* **110**, 11682 (1999).
- [47] Q. Wang and C. H. Greene, *Phys. Rev. A* **44**, 7448 (1991).
- [48] G. K. Jarvis, M. Evans, C. Y. Ng, and K. Mitsuke, *J. Chem. Phys.* **111**, 3058 (1999).
- [49] H. Lefebvre-Brion and R. W. Field, *Perturbations in the Spectra of Diatomic Molecules* (Academic, New York, 1986), Chap. 7.4.
- [50] D. Gauyacq, M. Raoult, and N. Shafizadeh, in *The Role of Rydberg States in Spectroscopy and Photochemistry*, edited by C. Sàndorfy (Kluwer Academic, Amsterdam, 1999), Chap. 13.
- [51] S. N. Dixit, D. L. Lynch, V. McKoy, and W. M. Huo, *Phys. Rev. A* **32**, 1267 (1985).
- [52] W. Y. Cheung, W. A. Chupka, S. D. Colson, and D. Gauyacq, *J. Chem. Phys.* **78**, 3625 (1983).
- [53] S. Guizard, N. Shafizadeh, D. Chapoulaud, M. Horani, and D. Gauyacq, *Chem. Phys.* **156**, 509 (1991).
- [54] K. Takazawa and H. Abe, *J. Chem. Phys.* **110**, 9492 (1999).
- [55] P. F. Bernath, *Spectra of Atoms and Molecules* (Oxford University Press, Oxford, 1995).
- [56] J. C. Castro, M. L. Zimmerman, R. G. Hulet, D. Kleppner, and R. R. Freeman, *Phys. Rev. Lett.* **45**, 1780 (1980).
- [57] A. F. Starace and G. L. Webster, *Phys. Rev. A* **19**, 1629 (1979).
- [58] U. Fano, *Phys. Rev. A* **22**, 2660 (1980).
- [59] N. Shafizadeh, M. Raoult, M. Horani, S. Guizard, and D. Gauyacq, *J. Phys. II (France)* **2**, 683 (1992).
- [60] U. Fano, *Phys. Rev. A* **2**, 353 (1970).
- [61] H. A. Bethe and E. E. Salpeter, *Quantum Mechanics of One- and Two-Electron Atoms* (Springer, Berlin, 1957).
- [62] P. Labastie, M. C. Bordas, B. Tribollet, and M. Broyer, *Phys. Rev. Lett.* **52**, 1681 (1984).
- [63] M. C. Bordas, M. Broyer, J. Chevalere, P. Labastie, and S. Martin, *J. Phys.* **46**, 27 (1985).